



BACHELOR GRADUATION PROJECT

# Maximum Power Point Tracking Topology, sensor and switch design

**Authors**

Y.K.L.M. Prevoo 1323113

M.G.P. Hovens 1361503

**Supervisor**

Dr. J. Popovic

Delft University of Technology  
Faculty of EEMCS

June 26, 2012

# Preface

This bachelor thesis is part of a report that consists of three different theses. Together, they form a technical report for the bachelor graduation project Maximum Power Point Tracking for Electric Automotive applications. This project was proposed by the Nuon Solar Team for the bachelor Electrical Engineering at the University of Technology Delft. Together with this report, a business plan was written for the course High Tech Startups together with an ethical essay for the sub course Ethiek in bedrijf.

This project will extensively explain the technical challenges that come with realizing a maximum power point tracker for solar vehicles. The titles of the three theses in the project are:

- Maximum Power Point Tracking  
Topology, sensor and switch design
- Converter Design for Maximum Power Point Tracking
- Maximum Power Point Tracking: Algorithm and Software  
Development

We would like to thank:

dr. Jelena Popovic, supervisor of our bachelor graduation project, for her technical as well as non-technical support.

Milos Acanski MSc, for his contributions to the project and help with the simulation models.

Kasper Zwetsloot, for his assistance with building, testing and debugging the prototypes.

The Nuon Solar Team for providing funding, data equipment and facilities for testing.

Delft, June 26, 2012

Yves Prevoo

Max Hovens

# Summary

The Nuna 6 is a solar racing vehicle that solely relies on solar energy from the sun. Every year, the team seeks ways to improve the performance of their car. One way to improve the performance is to maximize the power output of the solar panels on top of the car. Maximizing the power output can be done with a 'Maximum Power Point Tracker'. The aim of this thesis was to develop an improved, distributed 'Maximum Power Point Tracking'-system which optimizes the power efficiency of the solar panel array of the Nuna 6 solar racing vehicle.

To prove that the proposed distributed topology is more power efficient when compared to a central tracking topology, simulations of the total Nuna 6 electrical system were performed. Based on the simulation results, together with Nuna 6 specifications, a DC-DC boost converter was designed. Validation of the design was done by simulation with the Nuna 6 model. After validation, a breadboard proof-of-concept was built. The proof-of-concept was successfully tested and compared with earlier simulations. The system design process was evaluated and recommendations for further study and future real-life implementations were formulated.

The simulation results prove that the proposed distributed tracking system is as much as 40% more efficient in large insolation differences and 10% in small insolation differences. The system excels when insolation differs, however it is slightly less efficient when used with equal insolation on every panel. The developed proof of concept demonstrates a functioning maximum power point tracker and DC-DC boost converter. The power efficiency of the boost converter was found to be between 95.8% and 98.5%, with an efficiency of 97.1% for the rated input power of 200W.

# Contents

<b>Preface</b>	<b>i</b>
<b>Summary</b>	<b>ii</b>
<b>1 Introduction</b>	<b>1</b>
<b>2 Problem Analysis</b>	<b>3</b>
2.1 Problem definition . . . . .	3
2.2 Requirements . . . . .	5
2.2.1 Required conditions . . . . .	5
2.2.2 Preferred conditions . . . . .	5
2.2.3 Optional conditions . . . . .	6
<b>3 Related Research</b>	<b>7</b>
3.1 Distributed MPPT approach . . . . .	7
3.2 Power converters . . . . .	8
3.3 Sensors . . . . .	9
3.3.1 Current measurement . . . . .	9
3.3.2 Voltage measurement . . . . .	11
3.4 Switching elements and drivers . . . . .	12
<b>4 Topology &amp; function formulation</b>	<b>15</b>
4.1 System topology and simulation . . . . .	15
4.1.1 System topology and functional division . . . . .	16
4.1.2 Simulation . . . . .	18
4.1.3 Comparison simulation . . . . .	22
4.2 Subsystem functions and concepts . . . . .	26
4.2.1 Sensors . . . . .	26
4.2.2 Switching element . . . . .	29
4.2.3 Gate driver . . . . .	34



<b>5 Subsystem design</b>	<b>38</b>
5.1 Sensors . . . . .	38
5.1.1 Current sensor . . . . .	38
5.1.2 Voltage sensor . . . . .	44
5.2 Switching element . . . . .	45
5.3 Gate driver . . . . .	47
<b>6 Proof of concept</b>	<b>51</b>
6.1 Implementation . . . . .	51
6.2 Sensors . . . . .	53
6.2.1 Current sensor . . . . .	54
6.2.2 Voltage sensor . . . . .	54
6.3 Switching element . . . . .	54
6.4 Gate driver . . . . .	54
<b>7 Evaluation</b>	<b>57</b>
7.1 Efficiency Measurements . . . . .	57
7.2 Gate driving . . . . .	59
7.3 Sensors . . . . .	63
7.4 Control circuitry . . . . .	64
<b>8 Conclusion &amp; Recommendations</b>	<b>65</b>
<b>Bibliography</b>	<b>70</b>
<b>Glossary</b>	<b>71</b>
<b>List of figures</b>	<b>74</b>
<b>List of tables</b>	<b>75</b>
<b>Appendix A - MOSFET Calculator</b>	<b>76</b>
<b>Appendix B - Model Plotter</b>	<b>82</b>
<b>Appendix C - Brief of requirements</b>	<b>84</b>
<b>Appendix D - IRFSL4620 Efficiency Measurements</b>	<b>88</b>

# Chapter 1

## Introduction

Every other year, the Nuon Solar Team of the University of Technology Delft participates in a solar-powered car race, called the world solar challenge. New developments in solar energy technology drive the Nuon solar team to further improve the performance of their vehicle. However, harvesting solar energy comes with its own challenges. Solar panels are highly dependent on the conditions they are placed in. A few characteristics that influence the energy efficiency are temperature, humidity, incidence angle of the sunbeams and shading [1]. These phenomena cause the point at which the power produced is maximized (known as maximum power point, or MPP) to change, which could lead to a decrease in energy production of as much as 30% [2].

A major technological challenge is to track the maximum power point. This is done with so called maximum power point trackers (MPPTs). Since a few years, MPPTs are being developed to keep track of this power point. However, due to high research costs involved and the relatively low market adaptation, MPPTs are expensive and in most cases, not suited for application in a solar racing vehicle, because of the special needs of the racing vehicle. The Nuon solar team uses two of these MPPTs in their cars. This is a cost-effective decision, but has major disadvantages concerning energy production, since multiple solar cells have to be connected to one MPPT and therefore it can only track the worst power-point of the available cells. To overcome this issue, the solar team needs to have an individual MPPT per two panels to effectively maximize the energy production.

This thesis describes the process of the design and realization of the overall topology of the MPPT, the switching device and the associated driver for

the MPPT module. A proof of concept demonstrates the viability of the proposed system.

Composed of eight chapters in total, this thesis will first focus on the analysing the problem and the overall topology of the MPPT. In chapter 2 the problem is defined, simulated and the boundary conditions are set by use of the Nuna 6. Chapter 3 describes relevant research in this field and shows the current state-of-art. Chapters 4 and 5 describe the design process that was used to derive the optimal solution and justifies the concepts that were chosen to be used in the MPPT. Chapter 6 will present the proof of concept. In chapter 7 the design process will be evaluated, recommendations in accordance with the evaluation are formulated in chapter 8.

## Chapter 2

# Problem Analysis

This chapter will consist of a thorough analysis of the problem in section 2.1, after which the requirements for the MPPT will be set in section 2.2.

### 2.1 Problem definition

To convert sunlight into energy, the Nuon Solar Team makes use of solar panels that are 22.3% efficient. Although Australia is a sun-drenched country, clouds occasionally cover the sun from the solar panels, decreasing the light intensity on the solar panels. Another effect that affects the performance of a solar panel is temperature.

In figure 2.1, it can be seen that the power density of a solar panel decreases with increasing temperature. From figure 2.2 can be derived that the power density significantly decreases when there is less light shining on the solar panel.

The weather phenomenon is a hard phenomenon to predict. Since the power directly relates to the performance of the Nuon Solar Team at the world solar challenge, maximizing the output power of the solar panels is an important goal for the Nuon Solar Team. In the current system, the entire PV area, which is divided into 10 separate 'strings' of 10 serially connected panels each, is connected to two Maximum Power Point Trackers. Each maximum power point tracker is only able to track one power point, and it will be limited by the string that performs the worst. This means that when only one of the 5 strings on one of the power point trackers receives less light, all strings on that tracker are operated below their optimum power point, thus wasting energy that could be used to win the race.

In this thesis, the main question is:

*How to efficiently maximize the output power of the solar panels for the Nuna 6 racing vehicle, by using multiple Maximum Power Point Trackers?*

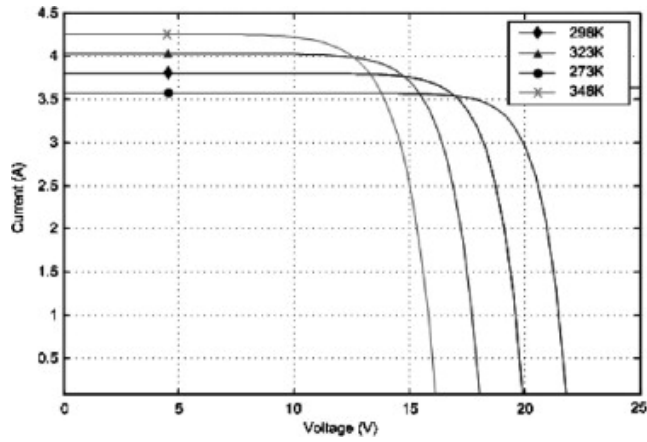


Figure 2.1: Temperature dependency of a solar panel, source: [3]

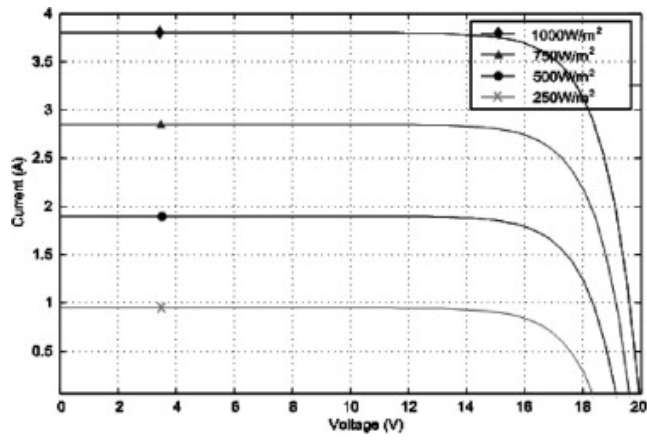


Figure 2.2: Light intensity dependency of a solar panel, source: [3]

## 2.2 Requirements

In this section, the requirements for the MPPT will be set. First the required conditions are set. These conditions must be met in order to produce a viable MPPT. The preferred conditions are the conditions that are not necessary for the project, but these conditions are common in MPPTs and should be added when possible. Optional conditions are the conditions for the end product, which will be put on the market, these conditions have the least priority. A more detailed overview of the requirements can be found in appendix C.

### 2.2.1 Required conditions

- The MPPT must have an efficiency of minimal 95%.
- The MPPT has to be installed in fivefold in Nuna's car, resulting in a nominal input power between 20W and 100W and an absolute maximum of 200W.
- The MPPT accepts input voltage between 60V and 120V and provides an output voltage between 120V and 160V.
- The MPPT provides plug-and-play connectivity, thus every team member of Nuna can install it.
- The MPPT needs to work independent, but must be able to react to externally given commands.
- The MPPT is maintenance-free during operation.

### 2.2.2 Preferred conditions

- The MPPT needs to communicate with the car using CAN-bus communication on a send-only basis, providing additional information on at least:
  - Power in [W]
  - Power out [W]
  - Input Voltage [V]
  - Output Voltage [V]
  - Output Current [A]

- An external reset switch is needed for resetting the MPPT during an infinite loop or error.
- Extra safety systems, such as fuses to prevent overcharging or limit short circuit damage are applied to the design.
- Input and output and other high-voltage connections need to be properly shielded.

### 2.2.3 Optional conditions

- The condition of the MPPT can be controlled visually using multiple leds.
- The design is robust, light and compact.
- The MPPT will work in the conditions given in Australia during the World Solar Challenge.
- All the used components meet the specifications as provided by Veolia World Solar Challenge.
- The case and connections are dust-sealed and are shock and vibration proof.

## Chapter 3

# Related Research

In this chapter the state-of-art is explored. First we will look at distributed maximum power point tracking in section 3.1, then in section 3.2 a general approach to power converters. Next, we will focus on the current and voltage sensors used in these systems in section 3.3, followed by the switching element in section 3.4 and the driver in section 3.4.

The Nuna Solar Racing car operates  $6m^2$  of PV panels that output a certain DC voltage. The engine and battery system of the car operate at another, higher, voltage. Furthermore, to operate the PV panels efficiently, they need to be kept at a specific voltage and current, using an algorithm. In order to set the PV panels at their maximum power point and provide the engine and batteries with the required voltage, a power conversion device is needed. To minimize the effects of partial shading and differences in solar incident angle, the total PV area is divided into several smaller segments. Each segment will be equipped with its own tracking unit and power converter.

### 3.1 Distributed MPPT approach

A drawback of solar panel arrays is the loss of power due to partial shading of the panels or mismatches in the PV modules themselves. Under ideal conditions, these losses are minimal or absent [4]. In these ideal conditions, the maximum power point for the whole array is the same. Under partial shading conditions there exist multiple power points, where the central tracker can only track one. Not all panels are operated at maximum power, and energy is lost. Distributed Maximum Power Point Tracking (DMPPT) aims to overcome these issues by giving each panel its own tracker, ensuring efficient operation of all panels [5]. In essence, going from a central Power



Point Tracker to DMPPT requires only the installation of more trackers on the same array. Having multiple trackers can increase cost, but these trackers require a lower power rating and therefore can be cheaper per piece than a large tracker. In most systems, the added cost of extra power electronics is outweighed by the gain in energy output [6]

### 3.2 Power converters

Power converters exist in several forms, and are ultimately derived from a general form of power supply. An overview of power supply technology is given in figure 3.1.

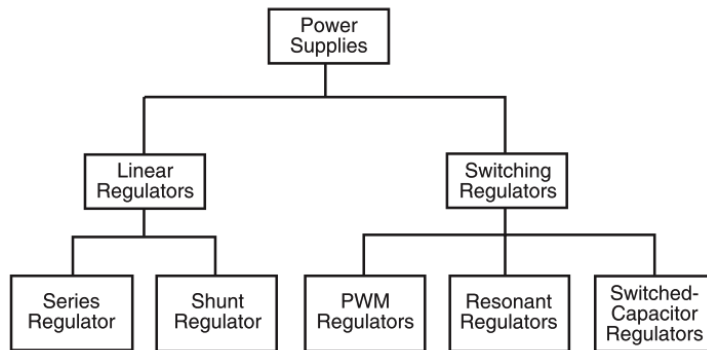


Figure 3.1: Classification of power supply technologies, source: [7]

From figure 3.1 we see that two classes of regulators exist, linear and switching regulators. Although linear regulators have excellent characteristics when it comes to bandwidth and noise, they can only step-down a voltage, [7], thus rendering them useless for our application where an increase in voltage is needed. Switching regulators come in three forms: switched-capacitor, resonant and Pulse Width Modulation (*PWM*) regulators.

Switched capacitor regulators, or charge-pumps, can be used to step-up a voltage without the need for inductors and with relative simple circuit topologies [8]. These types of converters see much use in level translators in digital communication buses and low power integrated step-up converters, however they are not suited for medium or high-power applications due to limitations on the capacitors [9, 10].

*PWM* regulators regulate their output voltage by hard switching a transistor between the on and off states, whereby the duty cycle of the switch

control signal determines the output voltage. A magnetic field in an inductive element is used to store and release energy, which also allows some types of PWM regulators to step-up the input voltage [7]. More efficient PWM converters are constructed by using soft-switching techniques, reducing the losses in the switch. Examples are converters that rely on resonance to switch under Zero-Voltage or Zero-Current conditions or snubber circuits that accomplish the same task. While these techniques can greatly improve converter efficiency, they also increase the complexity [11, 12, 13, 14, 15, 16, 17, 18].

### 3.3 Sensors

In order to calculate the maximum power point, we need to measure the current and voltage of the solar panel(s) that are connected to the maximum power point tracker. To do this, we will use voltage- and current sensors. In order to pick the right sensor, we will briefly describe the possibilities.

#### 3.3.1 Current measurement

Current can be measured in three different ways: resistive, optically isolated resistive and magnetically [19]. Each way of measuring current has its own advantages and disadvantages. The three ways of measuring current are compared in table 3.1 on a few key points.

Table 3.1: Common current measuring methods [19]

Type	Current range	Isolated	Accuracy	AC Response	Non-Intrusive	Cost
Resistive	Very low - High	No	High	Medium - High	No	Low
Optically isolated resistive	Medium - High	Yes	Low - Medium	Low - Medium	No	Medium
Magnetic	Medium - Very High	Yes	Medium	Medium - High	Yes	High

**Resistive** Resistive measurement or shunt measurement is a way of measuring current with the use of Ohms law. Shunt resistors are low value resistances that are placed in the path of the current. Because of this current a voltage is created across the terminals of the shunt, proportional to

the current value. Shunt resistors are low cost and easy to use. Often, a differential amplifier amplifies the voltage across the shunt to increase the signal-to-noise ratio. This setup can be found in figure 3.2. However, since the shunt is in-circuit, the efficiency of the system is reduced [20].

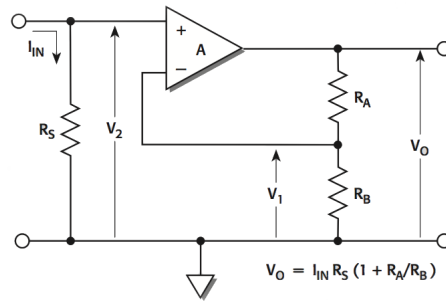


Figure 3.2: Shunt current sensor, source: [20]

**Optically isolated resistive** Optically isolated resistive current measurement is used in high-current systems (typically  $>100kA$ ). Due to complexity, size and price, optical sensors are not really a feasible option for us, so it will not be further investigated here.

**Magnetically** Magnetic current measuring can be done several ways [21]:

- Current transformer
- Rogowski coil
- Search-coil magnetometer
- Flux-Gate magnetometer
- Magneto diode
- Hall sensor

The first five measurement techniques have in common that they can only measure AC and therefore these forms are merely given as an example of ways to measure current. Since our system only operates on DC, we will not further discuss these measurement techniques.

**Hall sensor** The Hall sensor is a sensor that is based on the Hall effect. Discovered by Edwin H.Hall in 1879, it is the effect that a voltage is induced perpendicular to a current that is passing through a metal sheet, when a magnetic field is passing through the plate. The voltage is a result of the Lorentz force that acts on each individual charge particle that passes through the sheet; this force is perpendicular to the current and magnetic field.

### 3.3.2 Voltage measurement

Like current measurement, voltage measurement can be done in several ways. In table 3.2 several ways of measuring the voltage are given.

Table 3.2: Common voltage measuring methods [22]

Class	Operating principle	Subclass	Application field
Electromagnetic	Interaction between magnets and magnetic fields	Moving magnets	DC
Electrodynamic	Interaction between currents	-	DC and AC
Electrostatic	Electrostatic interactions	-	DC and AC
Thermal	Current thermal effects	Direct action	DC and AC
Induction	Magnetic induction	Analog	DC and AC
Electronic	Signal processing	Analog and Digital	DC and AC

As we can see from table 3.2 we can measure voltage in six different ways. However, electromagnetic, electrodynamic, electrostatic, thermal and inductive measurement of voltage are no feasible options for us, since they require mostly large components, moving parts or large currents, which in our case, are hardly applicable.

As shown in table 3.2, there are two ways to represent a measure of voltage: analogue and digital. In our MPPT, an analogue-to-digital converter (ADC) will be used. However, an ADC only accepts voltages in the range of 0 – 5V. Since our input voltage will be 60 – 120V we will have to scale the voltage,

prior to sending it into the ADC. Voltage scaling can be done in several ways: voltage division using resistors and an opto-coupled floating transformer.

**Voltage divider** A voltage divider is a simple serial connection between two resistors (shown in figure 3.3). Due to Kirchhoffs law, the voltage is divided between the resistors. This setup is simple to make, but it will reduce our resolution by a factor 2.

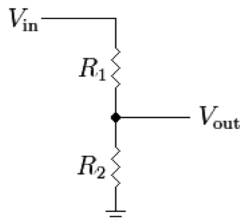


Figure 3.3: Voltage division

**Optocoupled floating transformer** An opto-coupled floating transformer first transforms DC to AC with an opto-coupler. This is then fed into a transformer that will decrease the primary voltage to a smaller voltage, a little bit larger than the desired voltage. At the secondary side of the transformer, the voltage will be rectified and divided again to give the appropriate value. The trick of this transformer is in the part that it uses a floating voltage as reference. Because of this, it will only decrease the voltage range that is informative to be measured.

### 3.4 Switching elements and drivers

Central to any of the mentioned power converters is the switching element. For any converter the choice is between a Bipolar Junction Transistor (*BJT*) Metal-Oxide-Semiconductor Field-Effect Transistor (*MOSFET*), Insulated Gate Bipolar Transistor (*IGBT*) or a *Thyristor*. Thyristors are not considered as they are not used in practice for our type of application. The choice between a BJT, MOSFET and IGBT remains and is made based on rated output power, voltage, operating frequency and efficiency: IGBTs are good devices for low-frequency, high-voltage, high-power applications [7] where the limit between low and high-power applications is generally put at 500 W [23]. Most IGBTs can be operated up to around 50 kHz, making them unsuitable for high frequency converters [24, 25]. Figure 3.4 shows the

preferred operating regions of IGBT or MOSFET switches, not taking the operating power into account.

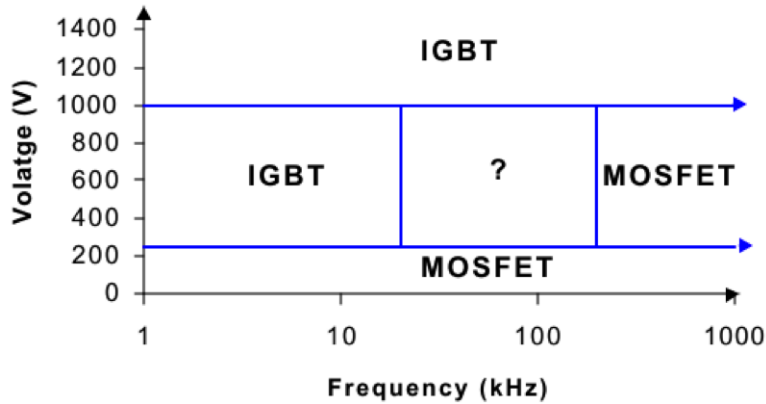


Figure 3.4: Preferred operating regions for MOSFET and IGBT, source: [23]

Figure 3.5 shows the operating regions of MOS devices versus BJT's. Figures 3.4 and 3.5 clearly show the advantage of MOSFET over IGBT and BJT devices, therefore, in this thesis we will focus on MOSFETS as switching devices as they are preferred in the operating range of the converter as described in Chapter 2.

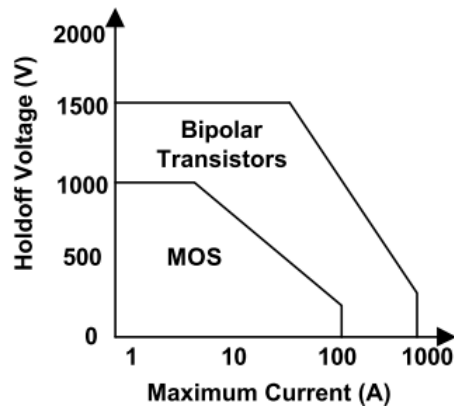


Figure 3.5: Preferred operating regions for MOSFET and BJT, source: [26]

**Gate driver** A drive circuit is needed to quickly switch the switching device between its on and off states, minimizing the time spent in the device's active region with relative high dissipative losses [27, 28, 29]. Control for the switch will be provided by a microcontroller operating at logic-level. The drive circuit acts as an interface between the digital logic and the MOSFET, amplifying the control signal and providing isolation between the two devices. The MOSFET is a voltage controlled device, requiring a constant voltage on the gate to remain conductive, however the presence of parasitic capacitances  $C_{gd}$  and  $C_{gs}$  greatly influences the behaviour of the MOSFET, requiring significant current to rapidly charge/discharge, needed to achieve the necessary fast switching times [30]. Currently, the use of dedicated gate driver chips is widespread, as they are easily available, relatively cheap and provide good performance [31, 29].

## Chapter 4

# Topology & function formulation

In this chapter the development of a first-order quantitative model for the electrical power system of the Nuna 6 Solar Racing Vehicle is described. With this model, different topologies can be simulated in order to find the most efficient solution regarding maximum energy output using a new type of MPPT + DC/DC converter. Section 4.1 describes the Nuna 6 system topology and describes the development of the model. In section 4.2, the system topology from 4.1 is broken down into sub-systems and their functions are explained. Then the chapter continues describing the process with which concept solutions for these functions are made and present equations used to justify the choices made in the final design.

### 4.1 System topology and simulation

In this section, the overall topology and the division into subsystems and further into functional elements will be made. A simple schematic overview of the Nuna 6 is shown in figure 4.1. For reasons of simplicity, only relevant modules are shown. The different components will briefly be discussed.



### 4.1.1 System topology and functional division

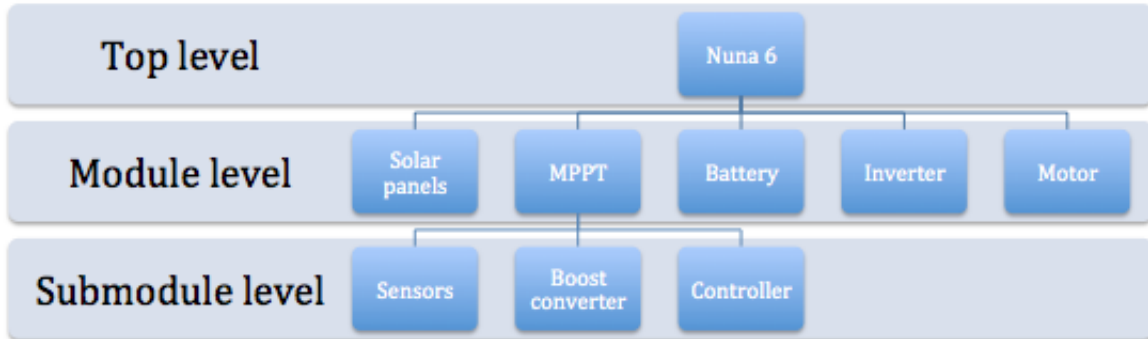


Figure 4.1: Total system overview of the Nuna 6

**Solar panel** The solar panel is the source of energy for the Nuna 6. Characteristics of the solar panel directly influence the performance of the Nuna 6. For the simulation, the Simulink model for a standard solar cell is used, which is defined according to the specifications of the solar cells of the Nuna.

**Motor** To drive, the Nuna uses an electric motor to propel the vehicle. This motor consumes most of the power, however it can also feed power back into the system using regenerative braking.

**Battery** As energy storage device, a battery is used. For simulation, a standard battery model is used, defined according to the specifications of the Nuna 6 battery.

**Inverter** The inverter, also called motor controller, converts the DC voltage from the battery pack into a three-phase AC voltage to drive the motor. It also allows power to flow from the motor into the battery, to enable regenerative braking.

**MPPT** Finally, the MPPT is modelled using submodules. The submodules are defined by their function. First to measure the current and voltages, a sensor submodule is implemented. Secondly, a boost converter is modelled, which will up convert the voltage. The controller is a submodule that is in between the boost converter and the sensor submodules. The

controller controls the conversion done in the boost converter, according to the information it receives from the sensor submodule.

To correctly control the converter, the controller needs a reliable and accurate measurement of the voltage and current of the input and output of the solar panel and MPPT, respectively. The sensor module can be divided in two elements (shown in figure 4.2). The two elements represent an individual function, which has its own specifications. These specification will be further developed in section 4.2.

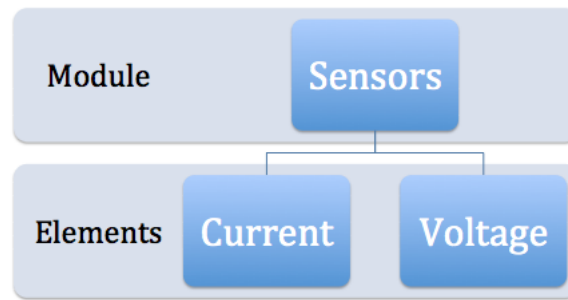


Figure 4.2: Division of sensor submodule into functional elements

To convert the voltage from the level of the battery, a converter is needed that can convert voltage up. To do this, a boost-converter is used. A boost-converter consist of four elements that each have their own function, as shown in figure 4.3. A switching element, switches an energy storage element that in turn, stores the energy that is delivered by the solar panel. Next a rectifying element rectifies the voltage that is created by the storage element. However, since the characteristic is AC, it needs to be smoothed to create a steady voltage at the output.

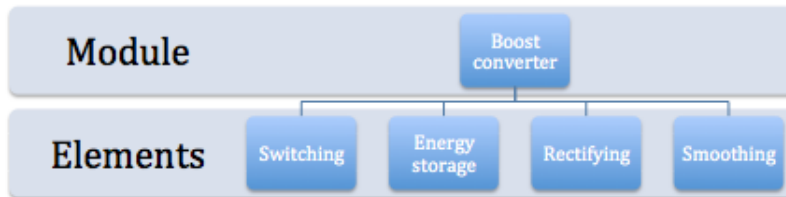


Figure 4.3: Division of boost converter submodule into functional elements

As last submodule of the MPPT, the controller is the brain of the MPPT.

It is fed the information of the sensor submodule, with which it calculates the maximum power point and then generates a pulse that controls the time the switching element of the boost-converter will stay on. The first stage in the information processing is the conversion from the analogue signal of the sensors to a readable, digital signal. Through an algorithm, the maximum power point is calculated. The last element, the PWM Generator then creates the signal that controls the boost-converter element, the switch. A schematic overview of the elements of the controller is given in figure 4.4.

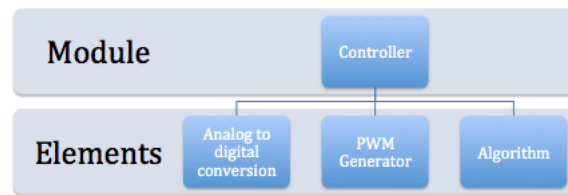


Figure 4.4: Division of controller submodule into functional elements

#### 4.1.2 Simulation

In order to test the MPPT before building it, a simulation is done of the real world scenario. In this simulation, assumptions are made to decrease the simulation time and increase the simplicity of the simulation. These assumptions are made because of the short time in which we have to perform the simulation. First, a model of the current setup of the Nuna 6 is developed, secondly a model with the proposed, new MPPT setup is constructed. Both models only differ in the number and type of MPPTs used and the arrangement of the solar panels. The current setup of the Nuna 6 contains DriveTek MPPTs and its model will be referred to as *Nuna 6 + DriveTek*. The MPPT designed in this thesis is called SolarMax. The model of the proposed system will therefore be referred to as *Nuna 6 + SolarMax*. Both models will be compared to each other based on performance in their power output.

**Software** For the simulations, Matlab and more specifically Simulink was used. Simulink was chosen for its comprehensive component libraries, flexibility and familiarity.

**Model** In this section, a model for the current Nuna 6 is developed. This model will be used as a reference for improvements. As we have seen in

figure 4.1, there are four Simulink submodels to be developed: a model for the solar panels, the MPPT, the battery and the motor. With each submodel the assumptions and simplifications will be given.

**Solar Panels** Solar panels are an array of serially connected solar cells. The Nuna solar panels have been modelled using the standard Simulink solar cell model. The parameters to this model have been adjusted to match the actual Nuna 6 cell parameters, which are SunPower C60 silicon cells. There are 25 panels on the Nuna 6, comprised of 8 different dimensions. The most common panel on the car, with 10 of the 25 panels being of this type, has been modelled. It contains 84 cells. Figure 4.5 shows a part of this setup. The only input to this system is the solar insolation in  $W/m^2$ .

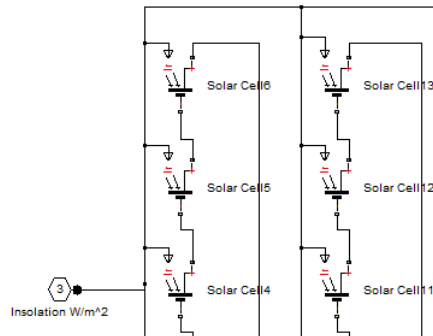


Figure 4.5: Partial solar panel model

*Assumptions & simplifications*

- The Simulink solar cell model is correct and applicable.
- The SunPower C60 cells can be modelled by fitting the datasheet parameters to the Simulink model.
- The solar insolation is constant over the panel.
- Temperature variations are not considered.

**DriveTek MPPT** The Nuna 6 currently contains a commercially available DriveTek V4 DC-DC Converter and maximum power point tracker. The components for this power converter have been reverse engineered from the system and put into the model. It should be noted that the output capacitors are much larger than what would be expected based on a minimal

ripple current [32]. This is possibly done in order to keep the output voltage as stable as possible. There could be some room for improvement here in the DriveTek design. Originally, the switching device in the converter was modelled using the SPICE model for the actual DriveTek MOSFET. This however proved to be computationally complex and it was replaced by a simple switch. The switching losses in the MOSFET are not taken into account, however the average conduction losses are modelled.

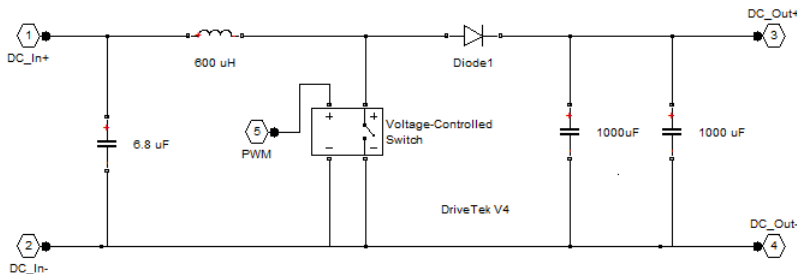


Figure 4.6: DriveTek V4 Converter model

The algorithm that controls the PWM signal is proprietary and unknown. A Perturb & Observe algorithm [33] will be used in the simulations. This is a highly popular algorithm as it is relatively simple yet very efficient.

#### *Assumptions & simplifications*

- The switching losses are left out.
- The control algorithm is replaced by Perturb & Observe.
- The inductor series resistance is assumed to be  $0.2 \Omega$ .

**SolarMax MPPT** The SolarMax MPPT is the DC-DC converter and maximum power point tracker discussed in this thesis. Its performance will be compared to the current system. The DC-DC converter has been modelled after design data provided by the authors and [32, 33]. As with the DriveTek, the exact MOSFET model has been removed.

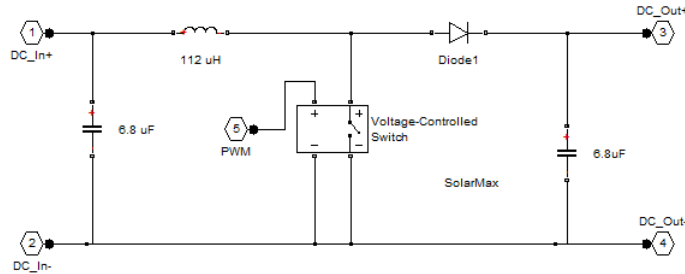


Figure 4.7: SolarMax Converter model

In order to keep the simulations practical, and to be able to compare the different systems, the same MPP algorithm as the DriveTek (Perturb & Observe) has been implemented. This way differences in the converter and the distributed MPPT setup can be simulated, but not the actual differences in performance of the different algorithms. For a detailed analysis of these performances, we refer to [33].

#### *Assumptions & simplifications*

- The switching losses are left out.
- The control algorithm is by Perturb & Observe.

**Battery** The Nuna 6 battery system consists of 38 serially connected battery strings, with each string containing 12 parallel batteries. In total, 456 Panasonic NCR18650A Li-Ion batteries are used. The battery bank has been modelled using Simulink’s Li-Ion battery model, where the parameters have been matched to the Nuna 6 setup, using [34, 35].

**Motor** The Nuna 6 uses a 3-phase AC motor to propel the vehicle. To convert a battery pack DC voltage to the motor 3-phase AC, a motor controller is used. Initially this system was modelled in a Simulink model containing the motor, modelled after the Nuna motor specifications and the motor controller. This system performed somewhat erratically and proved to be much too slow to simulate as part of a larger system. Therefore, the DC-AC conversion and motor were greatly simplified. Data provided by the Nuna team showed that under steady-state (cruise-speed) conditions, the average power consumption of the motor was about  $1.1kW$ . With a specified battery voltage of  $160V$ , the steady-state DC resistance of the motor can be

calculated. The motor submodel has thus been reduced to a single resistor, greatly speeding up the simulations, but eliminating the possibility to simulate vehicle acceleration or regenerative braking scenarios.

#### *Assumptions & simplifications*

- DC-AC conversion and advanced motor model have been left out.
- The vehicle has a constant cruise speed on a level surface.
- No transient analysis possible.
- The DC resistance of the motor is  $25\Omega$ .

### 4.1.3 Comparison simulation

In order to compare the current system and the proposed new setup, a comparison simulation has been done. The main problem of the current setup is that there are only two DriveTek MPPTs in the vehicle. Half of the solar panels are connected to one DriveTek MPPT. With different insolation on parts of the car, each panel might have a different maximum power point. Since each MPPT can only track one of these power points, the total efficiency decreases. By using multiple SolarMax trackers we decrease the amount of panels attached to each tracker and therefore can operate more panels on the true maximum power point. This simulation is meant to show the differences in power generation with the different setups.

**Nuna 6 + DriveTek** The *Nuna 6 + DriveTek* model consists of the Nuna 6 car elements, described in the previous paragraph, with two DriveTek trackers each with half of the solar panels connected to them.

**Nuna 6 + SolarMax** The *Nuna 6 + SolarMax* model has the same Nuna 6 car model as *Nuna 6 + DriveTek*, only it has four SolarMax trackers, each with  $\frac{1}{4}$  of the solar panels attached.

**Scenarios** Both models have been combined into one large model, and two scenarios have been simulated to compare the performance of both *Nuna 6 + Drivetek* and *Nuna 6 + SolarMax*. These models have been put together in one Simulink file for easy comparison, since they share the same inputs. Both models are run completely independently from each other within this

simulation, they only share common insolation input signals. This model is shown in figure 4.8.

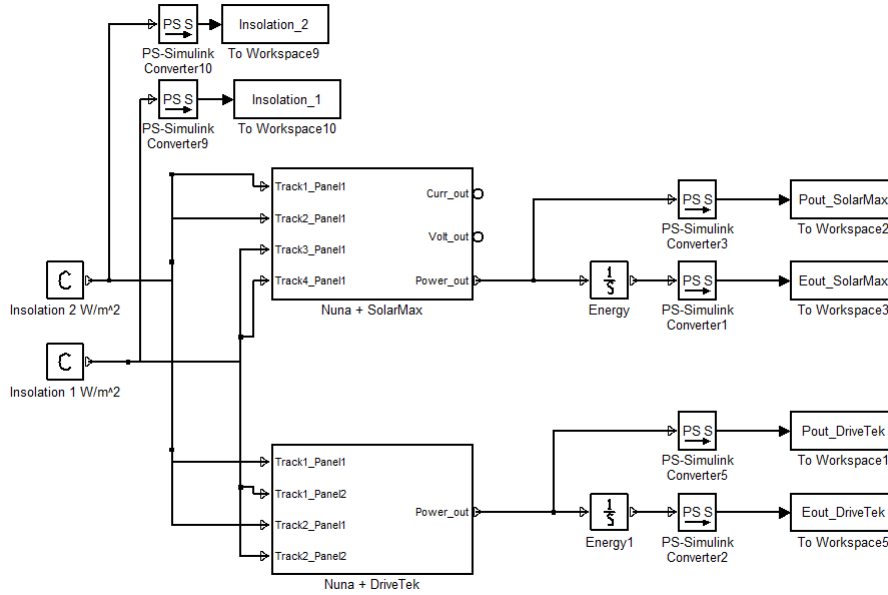


Figure 4.8: The complete combined model

The first scenario has equal insolation of  $1000W/m^2$  for all solar panels on the car. The results can be seen in figure 4.9.

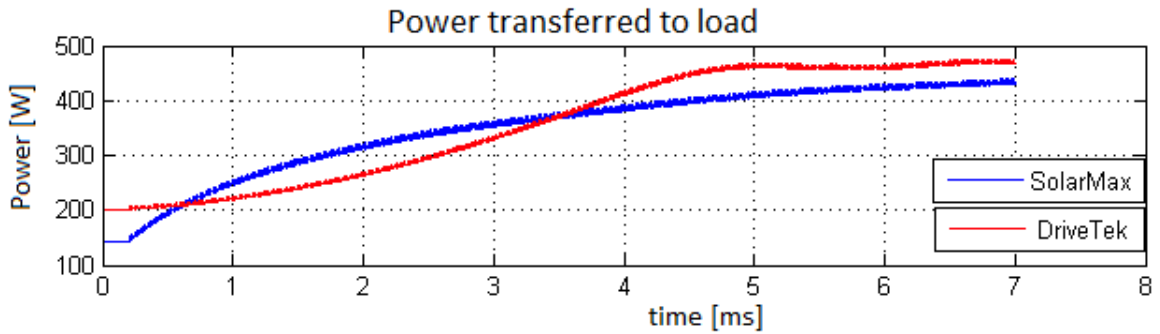


Figure 4.9: Output power for equal insolation of  $1000W/m^2$

We see that in the case of equal insolation, the DriveTek system performs



better than the SolarMax system. This is to be expected, as with equal insolation on all panels there is only one power point. The DriveTek system has only two MPPTs and therefore has lower converter losses than the SolarMax system, with its four MPPTs. We see that the SolarMax system tracks the power point faster than the DriveTek, but the stable output power of the DriveTek system is about 10% higher than that of SolarMax. Although the higher speed of SolarMax could be an advantage, this case proves that for equal insolation a central power point tracking solution would be best.

The second scenario has different insolation for half of the panels on the car. Originally, the idea was to simulate the insolation as a differing function of time for multiple different parts of the car, and then compare which system, *Nuna 6 + DriveTek* or *Nuna 6 + SolarMax* would yield the most energy. This would closely match the real-world scenario where partial shading (both slow and fast, e.g. clouds and roadside trees) and differing incident angles play an important role. However, it soon became apparent that this was computationally too demanding, with simulations taking multiple days to complete. To keep the simulation times manageable, the car has been split into two different segments of multiple panels, each with its own constant insolation. With the insulations set at  $1000W/m^2$  and  $2000W/m^2$ , we arrive at the results in figure 4.10.

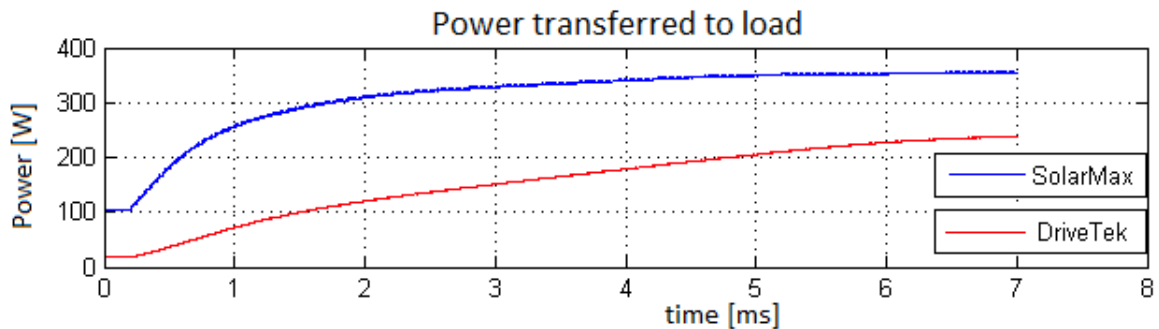


Figure 4.10: Output power for insolation 1000 and  $2000W/m^2$

We see in this case that after the tracking system has stabilized, the output power of the SolarMax system is roughly 40% higher in this simulation. It can also be seen that the DriveTek system takes longer to track the maximum power point. This could be due to the fact that there are more solar panels connected to one tracker. Although the differences in favour of the SolarMax

in this case are obvious, and the chosen insolation values are typical for race conditions, situations in which the insolation on one half of the car is twice as high as on the other half, might not be very common. Insolation values differing by a factor two could be of importance in areas with lots of trees or shrubs along the road. Under these conditions, the benefit of the SolarMax system are clear.

Another simulation with smaller differences in insolation, set at  $750W/m^2$  and  $1000W/m^2$  respectively, has been done. The results are shown in figure 4.11.

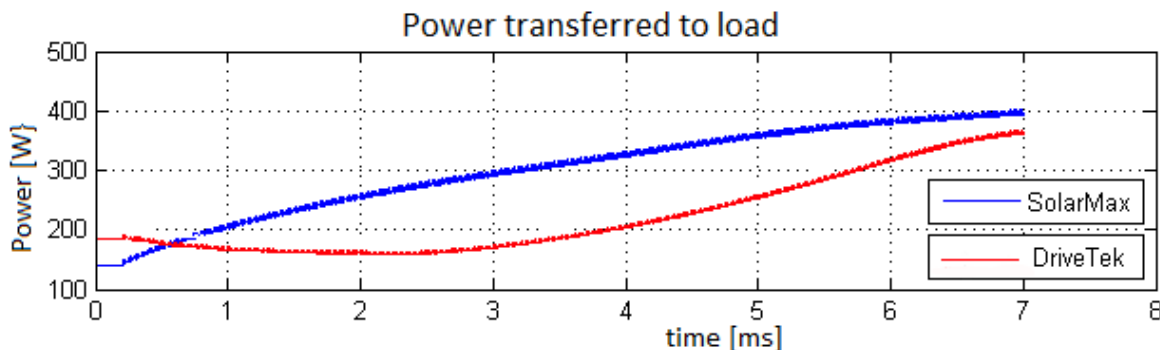


Figure 4.11: Output power for insolation  $750$  and  $1000W/m^2$

We see that the DriveTek system tracks the power point slowly and eventually settles at a total output power that is 10% lower than that of SolarMax.

These results prove the point that when the differences in insolation are less extreme (compared to the case above, which had  $1000$  and  $2000W/m^2$ ), the gain in efficiency is also less with a distributed system. However, a 10% gain in efficiency is very significant for the Nuna team and can easily mean the difference between winning and losing a race. Also, the faster tracking of the SolarMax system is significant in areas with quickly changing lighting conditions.

**Summary** These simulations prove that the proposed distributed maximum power point tracking topology indeed is more efficient compared to the current *Nuna 6 + DriveTek* setup. Larger differences in insolation on different parts of the car lead to bigger differences between the *Nuna 6 + DriveTek* and *Nuna 6 + SolarMax* systems. With the insolation on the car being  $1000W/m^2$  and  $2000W/m^2$  (a difference of 100%), the gain in output

power is as high as 40%. With the insolation at  $750W/m^2$  and  $1000W/m^2$  (a difference of 25%), the gain in power is 10%, which clearly is a significant increase for a high performance racing vehicle such as the Nuna.

## 4.2 Subsystem functions and concepts

### 4.2.1 Sensors

In this section, a more detailed explanation of the current and voltage sensors functions and topologies will be given. In the first part, consideration regarding the current sensor will be made. This will be followed by the topologies of the voltage sensor.

#### Current sensor

In this section, multiple topologies of current sensing will be presented and discussed.

**Current sensor problem** As can be seen from section 4.1, the central brain of the MPPT will be a microcontroller. This controller only accepts inputs as voltages, not as currents, therefore, directly inserting current into a microcontroller is not an option. This presents our first constrained: the current needs to be converted into a readable, quantity: a voltage. Another restriction of the current sensor is that it should be as efficient as possible.

**Methods** As described in chapter 3, current sensing can be done in several ways. The first way to measure current is by using an indirect quantity that is (ideally) linear related to the current.

An example of a linear relationship between current and another quantity is Ohms law, which relates voltage to current through a resistor. This method of current measuring satisfies the first requirement stated in the first paragraph, it converts the current into a voltage. Power dissipation in a resistor is represented by the formula:

$$P = I^2 * R \quad (4.1)$$

This equation shows that the power dissipation is quadratic related to the current and linear proportional to the resistance value. Since the input current is fixed, the resistance value has to be picked very small. This, however, presents another dilemma. Since the resistor will be picked very

small, the voltage drop across the resistor will be very small. Since the voltage has to be transported into the microcontroller, it is a very small signal, which means that it is very susceptible to noise, which is hard to measure with an ADC.

**Signal-to-noise** To overcome the issue of low signal-to-noise ratio, the voltage can be amplified using an amplifier. Multiple scenarios can be evaluated to do this. However, there exist a multitude of off-the-shelf ICs that are specifically designed to measure current, which operate on an external shunt resistor and subsequently amplifies the voltage to logic level (5V). Selection of the implementations will be discussed in chapter 5.

**Summary** A summary of the function and requirements of the current sensor.

Function: measuring the input and output current of the MPPT and making this value available for a microcontroller.

Requirements:

- High accuracy
- Low power dissipation
- Translate to readable voltage for microcontroller (0 – 5V range)

### Voltage sensor

In this paragraph, there will be made a general specification of the voltage sensor and the functions it should accomplish.

**Voltage sensing problem** Measuring voltage is easier to accomplish than measuring current, because it does not have the restriction of having to be translated to a different quantity, as was the case with current measurement. This greatly simplifies things. With voltage measurement there is, however, another challenge that has to be overcome. Microcontrollers only accept voltage inputs ranging from 0 to 5V. The output voltage levels of the MPPT range from 60 to 120V. This makes a direct coupling of the solar panel to the microcontroller impossible. To come up with a solution, we have to do the inverse operation as we did with the current sensor; we have to divide

the voltage. Voltage division can be done in two ways: DC-DC conversion and resistor division.

**Methods** DC-DC conversion could be used to convert the  $120V$  to a lower, usable value. This would mean that a DC-DC converter has to be used, this is impractical due to complexity and time issues and therefore not further discussed.

**Voltage divider** As last option, the voltage divider remains. This simple but practical solution has its advantages and drawbacks. The main advantage of a voltage divider is that it is very easy to implement, since only what is needed are two resistors. The disadvantages of a resistor divider are that it can be inefficient in terms of power consumption and even more disadvantageous is the reduction in resolution. This reduction of resolution occurs because our voltage always remains between two values,  $60V$  to  $120V$ . This means that the output of the voltage divider (as shown in figure 4.12) ranges only from  $2.5V$   $5V$ , which means that the resolution is reduced by a factor of two, since the range between  $0V$   $2.5V$  is never used.

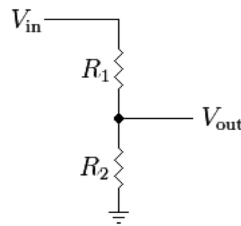


Figure 4.12: Voltage divider

**Summary** A summary of the function and requirements of the voltage sensor.

Function: measuring the input and output voltage of the MPPT and making this value available for a microcontroller.

Requirements:

- High accuracy
- Low power dissipation
- Translate to readable voltage for microcontroller (0-5V range)

### 4.2.2 Switching element

The switching element in DC-DC boost converter is preferably an ideal switch that switches between different current paths in the converter, as shown in figure 4.13.

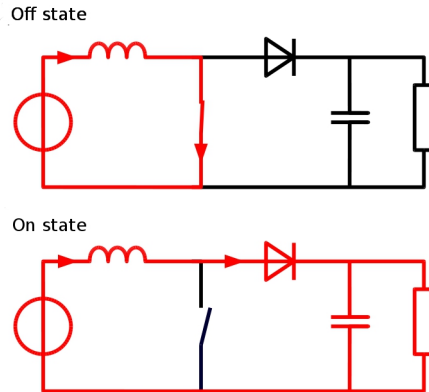


Figure 4.13: Boost converter topology, source: [36]

As this ideal switch does not exist, a real replacement for it has to be found that approximates the ideal conditions as close as possible. As we have seen in chapter 3, the choice for a switching device was already narrowed down by the available literature. A MOSFET is the device of choice because of its superior characteristics in the operating range of our converter. The process of designing, or selecting, a proper MOSFET is described below.

**MOSFET Considerations** When selecting a MOSFET, we first need to look at the requirements the device has to meet in order to function properly. Some theoretical background is given, and device selection is based on two separate groups of requirement: Requirements that ensure proper operation (*Operating requirements*) and requirements that reduce device losses as much as possible (*Performance requirements*). The basic requirements can be specified as a few fast rules that every device must absolutely meet: The MOSFET needs to be able to handle the peak inductor current. The Drain-Source voltage  $V_{DS}$  needs to be in excess of the output voltage + diode drop. The gate-source turn on voltage of the MOSFET,  $V_{GS}$  needs to be less than the input voltage (and never higher than the maximum allowed

$V_{GS}$  as specified by the manufacturer), to ensure that the voltage applied to the gate pin can actually turn on the MOSFET. Power dissipated in the device must be within the specified region. In order to ensure safe operation of the MOSFET, it needs to be operated within its specific safe operating area (SOA). The SOA is determined by three quantities intrinsic to the type of MOSFET used: Maximum drain current  $I_d$ , breakdown voltage  $V_{br}$  and junction temperature  $T_j$  [37]. The above parameters represent the bare minimum characteristics. However, to get a good design, we must ensure that the losses in the device are as low as possible. The MOSFET switch presents 2 losses in the circuit: switching losses and conduction losses. After the losses have been calculated, the thermal properties of the FET have to be taken into account, in order to ensure that the junction temperature does not exceed the rated value for the calculated dissipated power.

**Switching losses and switching speed** The switching behaviour of the MOSFET is largely affected by the various internal capacitors, shown in Figure 4.14.

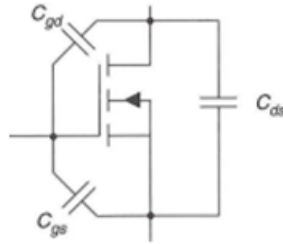


Figure 4.14: MOSFET with junction capacitance, source: [30]

The shown capacitances are non-linear parasitic capacitances influencing the device's operation. Specifically  $C_{gd}$  (also referred to as Miller capacitance, since its variations are caused by the Miller effect [38] and  $C_{gs}$  are strongly non-linear as a function of the input voltage, as shown in Figure 4.15.

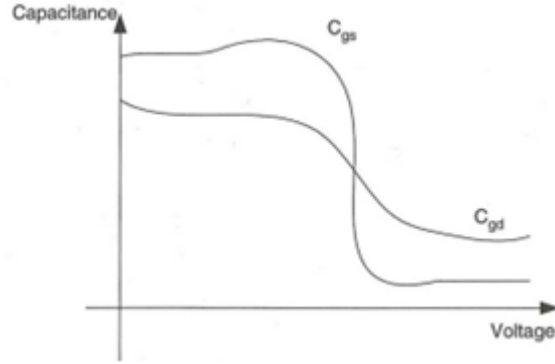


Figure 4.15: Variation of  $C_{gd}$  and  $C_{gs}$  as a function of  $V_{DS}$ , source: [30]

When the MOSFET is switched,  $C_{gd}$  and  $C_{gs}$  must be charged or discharged through the gate. This has strong implications on the choice for a proper gate driver circuit, as will be explained in the paragraph about drivers [30]. Switching losses in MOSFETs result from current flowing through the MOSFET at the same time that a voltage is across the device's terminals, during the turn on and turn off times of the MOSFET [27]. Small turn on and turn off times are thus required, not only to achieve the required switching speed, dictated by the operating frequency  $f_{sw}$ , but also to keep the losses to a minimum. One way to achieve this is to ensure low capacitances, where  $C_{gd}$  and  $C_{gs}$  are of particular importance [30]. The choice for a particular MOSFET will partially be based on the values for the capacitances  $C_{gd}$  and  $C_{gs}$ , however MOSFET manufacturers do not provide these values, but rather specify them as:

$$\begin{aligned} C_{gd} &= C_{rss} \\ C_{gs} &= C_{iss} - C_{rss} \\ C_{ds} &= C_{oss} - C_{rss} \end{aligned} \quad (4.2)$$

With  $C_{oss}$ ,  $C_{rss}$  and  $C_{iss}$  device parameters, provided by the datasheet [30]. To incorporate these various effects in choosing the right MOSFET, the total gate charge,  $Q_G$ , has become the figure of merit.  $Q_G$  makes for a handy, one-figure first look when selecting devices. Care must however be taken not to oversimplify things, since the test conditions provided by manufacturers might deviate and assumptions surrounding gate charge, specifically varying gate voltage, are only valid for specific conditions [31, 39]. Nevertheless,  $Q_G$  is a good tool in helping engineers efficiently selecting the right MOSFET. The following equations elaborate this: Charge is dictated by:



$$Q = I * T \quad (4.3)$$

Since  $f = 1/T$  where  $T$  is the period time, we can write:

$$Q * f = I \quad (4.4)$$

With (4.3) and (4.4) we can calculate the current needed to charge the gate capacitance of the FET. Since losses are the product of voltage and current, a high gate charge will lead to high dissipative losses in the driving circuit (see also next paragraph).

A first-order approximation of power loss due to switching in the MOSFET is given by [30, 31]:

$$P_{SWM} = \frac{1}{2} * V_{DS} * I_D * f_{sw} * (t_{rise} + t_{fall}) \quad (4.5)$$

With  $I_D$  drain current,  $f_{sw}$  switching frequency and  $t_{on}$ ,  $t_{off}$  the on and off times where finite values of  $I_D$  and  $V_{DS}$  co-exist, respectively.

**Conduction losses** Once the MOSFET has switched on, the MOSFET presents a small dc resistance between its Drain and Source terminals. This is the MOSFET's Drain-Source on resistance or  $R_{DS(on)}$ . Again, this needs to be as low as possible. Instantaneous power dissipation in the ON-state of the MOSFET is given by [27]

$$P_{CM}(t) = I_D^2(t) * R_{DS(on)} \quad (4.6)$$

Integrating 4.6 over  $T_{sw}$  gives the average of the conduction losses [40]:

$$P_{CM} = \frac{1}{T_{sw}} \int_0^{T_{sw}} P_{CM}(t) dt = R_{DS(on)} * I_{D_{rms}}^2 \quad (4.7)$$

With  $I_{D_{rms}}$  the *rms* value for the on state current, which for a boost converter topology is defined as [40]:

$$I_{D_{rms}}^2 = D * I_{in}^2 \quad (4.8)$$

We see that the conduction losses greatly depend on  $R_{DS(on)}$ , which is therefore an important parameter. MOSFET manufacturers reduce the on-resistance  $R_{DS(on)}$  of the MOSFET by constructing many parallel conduction paths between the drain and source. Thus, like connecting resistors

in parallel, the  $R_{DS(on)}$  comes down with more parallel paths. However, in connecting drain-source paths in parallel, a negative effect is that the gate-source capacitance  $C_{gs}$  is also connected in parallel, so a low  $R_{DS(on)}$ , and hence low conduction loss, implies a higher gate source capacitance with accompanying switching losses. Thus the MOSFET that is chosen should be a compromise between these two characteristics. In addition, high current MOSFETs tend to come in much larger packages, so meeting the ideal of low  $R_{DS(on)}$  and low  $C_{gs}$  might violate a space requirement specification. Another factor of importance is the fact that the  $R_{DS(on)}$  significantly increases with higher junction temperatures, because of an increase of charge carrier collisions, due to higher atom energies, and thus larger vibrations, in the semiconductor lattice structure [27]. Typical MOSFETs have a temperature coefficient from 0.35% to 0.5% [41]. The  $R_{DS(on)}$  at the operating temperature for the pessimistic temperature coefficient of 0.5% is given by [41]:

$$R_{DS(on)hot} = R_{DS(on)spec} * (1 + 0.005 * (T_{J(hot)} - T_{spec})) \quad (4.9)$$

where  $T_{spec}$  is the temperature at which  $R_{DS(on)spec}$  is specified.  $T_{J(hot)}$  is the designer's assumption of the MOSFET junction temperature.

Lastly, the  $R_{DS(on)}$  of a MOSFET inherently increases with an increase in breakdown voltage, because of the inverse relationships between breakdown voltage and  $R_{DS(on)}$  due to epitaxial thickness and doping levels [30] where low doping and high thickness represent a high breakdown voltage, but poor  $R_{DS(on)}$  and vice versa.

**Leakage losses** Next to both mentioned losses, there are also leakage (blocking) losses. When the MOSFET is in the off-state, it carries a small leakage current. As this current is in the  $\mu A$  range for a typical device [40, 7] these losses are usually neglected.

**Loss budget** The complete loss in a MOSFET is the sum of conduction and switching losses, neglecting the leakage losses and can now be computed using equations 4.7 and 4.5:

$$\begin{aligned} P_M &= P_{cond} + P_{SW} \\ P_M &= R_{DS(on)hot} * I_{Drms}^2 + \frac{1}{2} * V_{DS} * I_{Drms} * f_{sw} * (t_{on} + t_{off}) \end{aligned} \quad (4.10)$$

**Thermal management** The lost power from 4.10 is dissipated to heat that increases the junction temperature  $T_J$ . For each MOSFET, the maximum junction temperature,  $T_{Jmax}$ , is specified. Care has to be taken to ensure that this temperature is not exceeded, for silicon devices,  $T_{Jmax}$  is usually between 150 °C and 200 °C [7]. The temperature rise of the MOSFET junction relative to the ambient temperature,  $\Delta T_{JA}$ , is defined as [42, 7]:

$$\Delta T_{JA} = \theta_{JA} * P_D \quad (4.11)$$

with  $P_D$  the dissipated power and  $\theta_{JA}$  the thermal junction-to-ambient resistance. When a heatsink or other cooling element is applied,  $\theta_{JA}$  is [7]:

$$\theta_{JA} = \theta_{JC} + \theta_{CS} + \theta_{SA} \quad (4.12)$$

where  $\theta_{JC}$  is the manufacturer specified MOSFET junction-case thermal resistance,  $\theta_{CS}$  the case-to-sink thermal resistance and  $\theta_{SA}$  the sink-to-ambient thermal resistance.

The maximum power dissipation for a given  $T_{Jmax}$  and  $T_A$  is given by [7]:

$$P_{Dmax} = \frac{T_{Jmax} - T_A}{\theta_{JA}} \quad (4.13)$$

In order to calculate whether natural convection provides enough cooling, or if a heatsink is required, we can use 4.13 to calculate if the required  $\theta_{JA}$  can be met by the device.  $P_{Dmax}$  must be calculated using 4.7 and 4.9, where assumptions for  $T_{Jhot}$  have to be made.

**Device selection** The selection procedure for a particular device can now be based on the previous theory. First, the device has to meet the *Operating requirements*, and from the possible choices that remain, a trade-off between the *Performance requirements* has to be made. The  $R_{ds(on)}$  and  $Q_g$  hereby form the focus point, as they provide a relatively easy way to compare devices and they characterize the conduction losses and the switching losses in an obvious way. Using the design parameters, the dissipated power and the junction temperature can be derived. Based on this, a suitable MOSFET and possibly a heatsink can be selected.

### 4.2.3 Gate driver

The gate driver (also called switch driver or driver) provides the interface between the control circuitry and the DC-DC converter. Its function is to

ensure that the MOSFET is switched on and off fast enough based on the digital control signal. The MOSFET and driver are closely related and in their functionality strongly dependent on each other. The characteristics of the driver have to be carefully matched to those of the device it drives. Here we will present the procedure used to achieve this. As we have seen in chapter 3, the ability of the driver to charge/discharge the gate capacitance  $C_g$  is of utmost importance for achieving acceptable switching speed as well as limiting the switching losses. The typical MOSFET gate charge  $Q_G$ ,  $C_G$  and power required to charge this capacitance are related as [39, 29, 28]:

$$Q_G = C_G * V_{GS} \quad (4.14)$$

$$P_G = \frac{1}{2} * C_G * V_{GS}^2 * f_{sw} \quad (4.15)$$

First-order approximation for the power dissipated in the driver[39]:

$$P_D = C_G * V_{GS}^2 * f_{sw} \quad (4.16)$$

The time required to charge  $C_G$ , using a constant charge current,  $I_{charge}$ :

$$Q_G = I_{charge} * t_{charge} \quad (4.17)$$

with  $t_{charge}$  the charge/discharge time, as dictated by the switching time. This method is flawed however, as it does not take into account intrinsic properties of the driver circuit and assumes a constant charging current,  $I_{charge}$ , which is not the case. As we have seen in Figure 4.15, the capacitances change during the charge cycle. As  $V_{DS}$  decreases, the capacitance increases and the challenge for the driver circuit is to both charge  $C_{gd}$  and  $C_{gs}$  while their capacitance increases rapidly. As a rule of thumb, it is advised to select a driver circuit with a peak current rating  $I_{peak}$  of at least twice the calculated  $I_{charge}$ . We will see some enhancements to this crude method later in this chapter.

**Switch driver for Boost Converter** In the case of a simple boost converter as is described in this thesis, the switch element is directly tied to ground, allowing for a relative simple low-side gate driver circuit, eliminating the need for bootstrapping/charge pumping or other level shifting techniques associated with high-side driving [37]. Drivers can be designed from the ground up, using discrete elements, or an off-the-shelf IC driver can be chosen. IC drivers excel in convenience, compactness, low propagation delays and reliability, but lack the flexibility of a purpose-built circuit

which exactly matches the requirements [28]. A typical MOSFET driver is depicted in figure 4.16, showing a typical topology using a totem-pole output stage, using a P-MOSFET for charging and N-MOSFET for discharging the gate connected to the output.

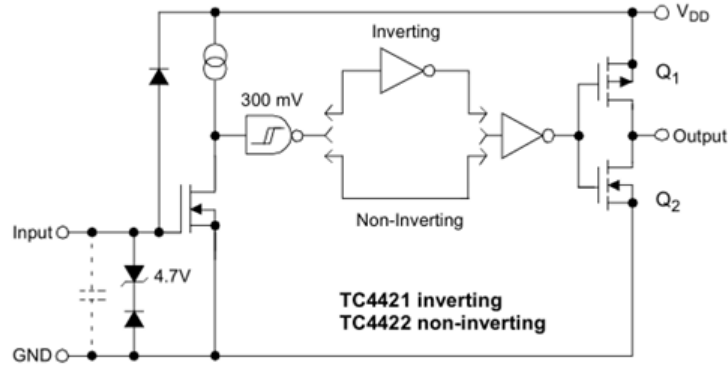


Figure 4.16: Microchip T442X 9A MOSFET Driver, source: [29]

In the transition state between charging and discharging, current flowing through Q1 is divided between the gate of the output MOSFET and Q2, leading to so-called shoot-through current, which in turn leads to dissipation usually named cross-over energy. When the gate is being charged, the circuit of figure 4.16 can be simplified to figure 4.17.

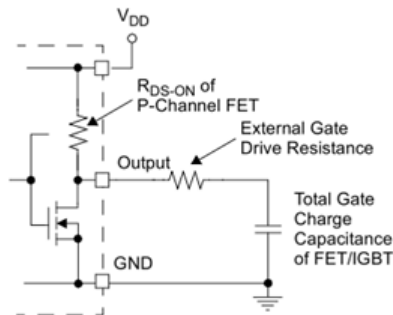


Figure 4.17: Microchip T442X charging external gate, source: [29]

This model allows us to revisit 4.16, making a more thorough analysis for selecting the right driver possible, based on a time constant approach [29]:

$$t_{charge} = (R_{driver} + R_{gate}) * C_G * TC \quad (4.18)$$

Where  $R_{driver}$  is the  $R_{DS(on)}$  of the drivers output stage P-MOSFET,  $R_{gate}$  any resistance between the driver output and the MOSFET gate and TC, the number of required time constants, which will range between 1 (63% charged) to 3 (95% charged), depending on the threshold voltage  $V_{TH}$  of the selected power MOSFET. It can be seen that through 4.3  $V_{GS}$  is taken into account, making for a more accurate selection based not only on  $I_{peak}$ , which is a rather simple figure used for easy comparison, but also on the required  $R_{driver}$  and  $V_{GS}$ .

With this more advanced driver model the dissipated power loss in the driver can be specified further compared to equation 4.16 [31]:

$$P_D = P_{D(on)} + P_{D(off)} \quad (4.19)$$

$$P_{D(off)} = \frac{(1 - D) * R_{OL} * V_{CC} * Q_G * f_{sw}}{R_{OL} + R_{gate}} \quad (4.20a)$$

$$P_{D(on)} = \frac{D * R_{OH} * V_{CC} * Q_G * f_{sw}}{R_{OH} + R_{gate}} \quad (4.20b)$$

Where:

$D$  = Duty cycle

$V_{CC}$  = Driver supply voltage

$R_{OH}$  = Driver output resistance with output high.

$R_{OL}$  = Driver output resistance with output low.

Combining equations 4.18, 4.17 and 4.19 allows us to combine all important properties of the MOSFET and driver and enables to choosing of a device that meets the specifications on  $I_{charge}$ ,  $I_{peak}$ ,  $R_{driver}$ ,  $t_{charge}$  and  $P_D$ .

# Chapter 5

## Subsystem design

In this chapter the design choices are presented and explained, based on the theoretical concepts from chapter 4. In a sense, this chapter describes the translation between theory and the practical application in order to build a functioning proof of concept. The designs are presented in the same order as the subsystems were developed in chapter 4. In section 5.1 the sensor modules will be designed, where after in sections 5.2 and 5.3, the switching element and gate driver will be designed.

### 5.1 Sensors

In the previous chapter, the overall functions of every subsystem were defined and the requirements for each subsystem were set. In this chapter, based on the requirements and functions, design choices are made and possible implementations are considered.

#### 5.1.1 Current sensor

As stated in chapter 4 the current sensor requirements were:

- High accuracy
- Low power dissipation
- Translate to readable voltage for microcontroller (0 – 5V range)

In the previous chapter, considerations were made about certain topologies. Here the topologies will be investigated further and the full implementation will be realized.

To attain high accuracy current sensing with a shunt resistor, a high value resistor would be most effective, since high value resistors create a high voltage drop across the shunt resistor, which results in a high signal-to-noise ratio. As we have seen from the previous chapter, this presents a dilemma with the power dissipation. A trade-off will have to be made. In practice, low shunt resistor values are used. The voltage across the shunt is amplified by an amplifier, which is subsequently fed into the microcontroller.

**Constraints** The first design challenge is to choose for high-side or low-side injection. High-side injection puts the shunt resistor into the hot wire of the system, whereas low-side injection puts the shunt into the ground wire of the system. High-side injection poses the problem that the shunt resistor and consequently the IC have to deal with large common-mode signals. On the other hand, low-side injection creates an undesirable resistor into the ground path, which creates a floating ground, which means that it needs a common-mode input range of below zero.

Due to ground complications with low-side injection, high-side is preferred. To implement the current sensor circuit, a decision can be made to implement and off-the-shelf IC or to implement a discrete operational amplifier. Implementing an discrete operational amplifier has some major disadvantages [43]:

- Low input resistance
- Common-Mode Rejection Ratio (CMRR) decreases very rapidly when resistors are not matched very well, which requires high precision resistors.

The Common Mode Rejection Ratio (CMMR) can be expressed in the following equation:

$$CMRR = 20 * \log_{10}\left(\frac{A_d}{A_{cm}}\right) \quad (5.1)$$

Where  $A_d$  is the differential gain factor and  $A_{cm}$  is the common mode gain factor, which is typically much smaller than the differential gain factor. For CMRR applies: the higher, the better.

Another constraint that is placed on the IC selection is the voltage the IC works on. In the brief of requirements in chapter 3 it is stated that the maximum input voltage will be 120V maximum and the output voltage will be 160V. So an IC is needed that can cope with these voltage levels.



Table 5.1: Current Sense IC overview

Name	Voltage range (V)	CMRR (dB)	High/Low-side
AD8212	+7 to > +500 with ext. transistor	80 at 10kHz	High-side
INA210	-26 to +26	140	Low-side
HV7801	-0.5 to +450	Not specified	High-side

**IC selection** The ICs that can be used are shown in table 5.1.1. Since high-side injection is preferred over low side injection, the INA210 is only to be taken as back-up solution. The two remaining ICs are further investigated.

The HV7801 is a high-side injection current monitor IC, which transfers a current measurement voltage value to its ground referenced output. This IC has a very wide input voltage range, high accuracy, low power consumption, ease of use, and low cost [44]. However, the CMRR is no-where specified, so this option is secondary to the AD8212.

The AD8212 is a high voltage, current monitor. It accurately amplifies a small differential input voltage in the presence of large common-mode voltages up to > 500V with an external PNP transistor. The current output of the device is proportional to the input differential voltage. The desired gain can be set with an external resistor. The feature that makes the AD8212 very useful is high voltage operation, which is achieved by using an external high voltage breakdown PNP transistor. In this configuration, the common-mode range of the AD8212 is equal to the breakdown of the external PNP transistor. Therefore, operation at several hundred volts is easily achieved. Because of the suitable characteristics, the AD8212 is a good choice; some calculations need to be made to incorporate this device into the MPPT.

**AD8212** A load current flowing through the external shunt resistor produces a voltage at the input terminals. As shown in figure 5.1, amplifier  $A1$  responds by causing  $Q1$  to conduct current through Resistor  $R1$  to equalize the potential at both the inverting and non-inverting inputs of  $A1$ . The emitter-current through  $Q1$  ( $I_{out}$ ) is proportional to the input voltage ( $V_{sense}$ ) and therefore is proportional to the current ( $I_{load}$ ) through the shunt ( $R_{shunt}$ ). By use of an external resistor the output current ( $I_{out}$ ) is converted

to a voltage. The output voltage value is dependent on the input/output gain equation desired in the application.

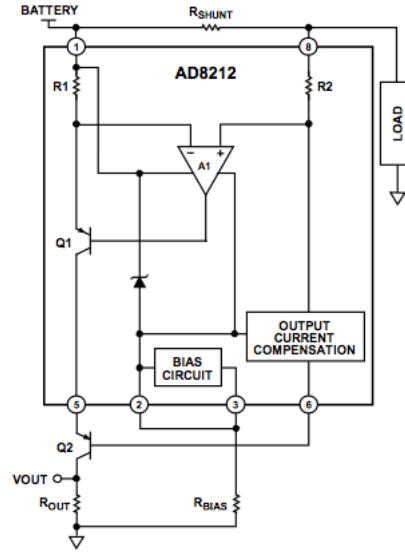


Figure 5.1: AD8212 Topology, source: [45]

**Shunt resistor** Calculating the resistor values for the required operating range [45]:

$$g_m = 1000 \frac{\mu A}{V}$$

$R_{out} = 100k\Omega$  for both in and output sensor, as given in [45].

$$\begin{aligned} I_{out} &= g_m * V_{sense} \\ V_{sense} &= I_{load} * R_{shunt} \\ V_{out} &= I_{out} * R_{out} \\ V_{out} &= \frac{V_{sense} * R_{out}}{g_m} \end{aligned} \quad (5.2)$$

$I_{load,in} = 3,33A$  at  $60V$ .

$I_{load,out} = 1,66A$  at  $120V$ .

Using equation 5.2,  $R_{shunt}$  can be determined.

$$\begin{aligned}
V_{out} &= \frac{V_{sense} * R_{out}}{g_m} = 5V \\
R_{shunt} &= \frac{V_{out} * g_m}{I_{load} * R_{out}} \\
R_{shunt,in} &= 0,015\Omega \\
R_{shunt,out} &= 0,030\Omega
\end{aligned} \tag{5.3}$$

Power rating calculation:

$$\begin{aligned}
P_{shunt} &= I_{shunt}^2 * R_{shunt} \\
P_{shunt,in} &= 3,33^2 * 0,015 = 0.166W \\
P_{shunt,out} &= 1,66^2 * 0,030 = 0.083W
\end{aligned} \tag{5.4}$$

**External transistor** The AD8212 has a 5V regulator. This regulator ensures that *COM* (which is the most negative of all the terminals) is always 5V less than the supply voltage ( $V_+$ ). Assuming a  $V_+$  of 120V maximum, it follows that the voltage at *COM* is:

$$V_+ - 5V = 115V \tag{5.5}$$

The base-emitter junction of *Q2*, in addition to the internal  $V_{be}$ , makes the collector of *Q1* approximately equal to:

$$115V + 2 * V_{be(Q2)} = 115V + 1.2V = 116.2V \tag{5.6}$$

This voltage appears across *Q2*. The voltage across *Q1* then is:

$$120V - 116.2V = 3.8V \tag{5.7}$$

This way, *Q2* resists 116.2V and *Q1* only 3.8V, which is below the breakdown voltages for each transistor.

**Bias resistor** Operating the AD8212 with an external transistor, means that  $I_{bias}$  increases as the input  $V_+$  increases. To chose the correct value for  $R_{bias}$ , figure 5.2 is used.

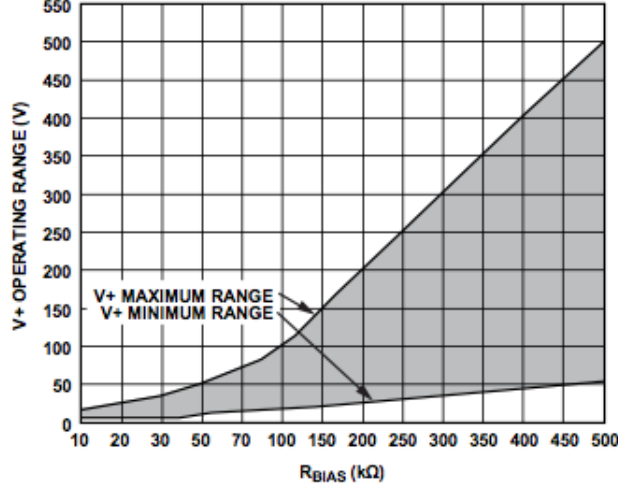


Figure 5.2: AD8212 Bias resistor chart, source: [45]

Since the maximum input voltage will be  $120V$ , the resistor value for  $R_{bias,in}$  should be about  $130k\Omega$ . The maximum output voltage is  $160V$  which means that we need a  $R_{bias,out}$  of  $170k\Omega$ .

$$\begin{aligned}
 I_{bias,in,max} &= \frac{120V-5V}{R_{bias}} = \frac{120-5}{130k\Omega} = 884\mu A \\
 I_{bias,in,min} &= \frac{60V-5V}{R_{bias}} = \frac{60-5}{130k\Omega} = 423\mu A \\
 I_{bias,out,max} &= \frac{160V-5V}{R_{bias}} = \frac{160-5}{170k\Omega} = 912\mu A \\
 I_{bias,out,min} &= \frac{120V-5V}{R_{bias}} = \frac{120-5}{170k\Omega} = 676\mu A
 \end{aligned} \tag{5.8}$$

From [45], it is recommended to maintain  $I_{bias}$  between  $200\mu A$  and  $1mA$  to ensure that the circuit operates as expected. With a  $R_{bias}$  of  $130k\Omega$ , the operation range is  $423 - 884\mu A$  for the input sensor and  $676 - 912\mu A$  for the output sensor. These values are well in the specified recommended range. Shown in figure 5.1,  $Q2$  can be a FET or a bipolar PNP transistor. The PNP transistor is less expensive, however  $I_{out}$  is reduced by the current lost through the base of the  $Q2$ . This will lead to an output error in the voltage over  $R_{out}$ . Fortunately, the AD8212 incorporates a current compensation circuit, which compensates for the loss of current in the base of the PNP transistor. The choice for a suitable PNP transistor is based on a high breakdown voltage,  $V_{ceo}$ , ( $> 120V$ ). We chose the BF423ZL1G due to its

high  $V_{ceo}$ , its low price and high availability.

### 5.1.2 Voltage sensor

As stated in chapter 4 the current sensor requirements were:

- High accuracy
- Low power dissipation
- Translate to readable voltage for microcontroller ( $0 - 5V$  range)

A decision was made in chapter 4 to incorporate an voltage divider because of ease of design. However, it came with the disadvantage of reducing the resolution by a factor 2.

There are a few design challenges when designing a voltage divider. As stated above power consumption must be reduced to a minimum, the resistors used should be linear over a sufficient voltage and current range, should be linear with increasing temperature and should be rated higher than the maximum power level, for safety reasons.

**Resistor values** Calculating the resistor values of the voltage divider, a constraint on the power dissipation has to be made. The power dissipated by a resistor is given by:

$$P_{diss} = \frac{U^2}{R} \quad (5.9)$$

From this equation, it is apparent that higher resistor values dissipate less power. As acceptable value, 0.05% of the total power was chosen. This is about  $0.1W$ .

As stated in chapter 4 the maximum output voltage should be  $5V$ , because of the microcontroller. This means that we have to scale down the voltages of the input and output of the MPPT, by a factor:

$$\begin{aligned} c_{u,in} &= \frac{R_1}{(R_1+R_2)} = \frac{5}{120} \\ c_{u,out} &= \frac{R_3}{(R_3+R_4)} = \frac{5}{160} \\ 23 * R_1 &= R_2 \\ 31 * R_3 &= R_4 \end{aligned} \quad (5.10)$$

With the power requirement stated as above ( $0,1W$ ), we can calculate the resistor values.

$$\begin{aligned} P_{diss,in} &= \frac{U^2}{(R_1+R_2)} \\ P_{diss,out} &= \frac{U^2}{(R_3+R_4)} \end{aligned} \quad (5.11)$$

$$\begin{aligned} R_1 &= 6k\Omega & R_2 &= 138k\Omega \\ R_3 &= 8k\Omega & R_4 &= 248k\Omega \end{aligned} \quad (5.12)$$

**Power rating** These resistors should all have a power rating of  $> 0.1W$ , with the smallest possible tolerance. For the resistors, the choice was made for  $0,25W$  resistors with a tolerance of  $0,1\%$ .

Since the microcontroller is very susceptible to higher voltages, a decision was made to put Zener diodes across  $R_1$  and  $R_3$  with a breakdown voltage of  $5V$ . If the input or output voltage increase to higher values than  $120V$  and  $160V$  respectively, the total voltage will fall across resistors  $R_2$  and  $R_4$ . This has consequences for the power rating of  $R_2$  and  $R_4$ . When choosing for  $0,25W$ , which have good tolerance factors, the maximum allowable voltage is:

$$\begin{aligned} U_{in,max} &= \sqrt{P_{max,R2} * R_2} = 185V \\ U_{out,max} &= \sqrt{P_{max,R4} * R_4} = 248V \end{aligned} \quad (5.13)$$

This means that for the input voltage a  $50\%$  of increase above the maximum voltage is survivable. For the output voltage this is  $55\%$ .

## 5.2 Switching element

With the theory developed in the previous chapter a well founded decision for the switching element can now be made. First, the *operating requirements* are set, secondly the *performance requirements* and lastly the practical considerations in selecting a device that meets the requirements are discussed.

**Operating requirements** These parameters, summarized in table 5.2, represent the absolute minimum the device must cope with.

- The minimum breakdown voltage  $V_{DS(br)}$  must be at least equal to the maximum output voltage,  $V_O$ . This value is derived from the Nuon Solar Team specifications.

- The continuous drain current  $I_D$  must be at least equal to the peak switch current  $I_{sw(peak)}$ , calculated in cooperation with the other design teams [33, 32].
- The total turn-on time  $t_{ton}$  and turn-off time  $t_{off}$  determine the maximum switching frequency. With the switching frequency set at 100 kHz, the total cycle time of the MOSFET is maximum 10  $\mu$ s. We will see that this is not a limitation, as all devices can be operated at much higher frequencies.

Table 5.2: MOSFET Operating requirements

Parameter	Minimum	Typical	Maximum
Drain-Source breakdown voltage $V_{DS(br)}$	160 V	200 V	no limit
Continuous Drain Current $I_D$	3.9 A	5 A	no limit
Total cycle time $t_{cycle}$	no limit	-	10 $\mu$ s

**Performance requirements** In the design process we saw that the total losses in a MOSFET depend on a trade off between several parameters. The  $R_{DS(on)hot}$ ,  $Q_G$ , and thermal properties are of most importance.

**Device selection** All components were selected from Farnell, on request from the Nuon Solar Team. Using their parametric search function, all components that do not match the *Operating requirements* were filtered out. Also, all components not in stock or in surface-mount packages were not considered, due to time limitations. The remaining components need to be selected on their *Performance requirements*. For the selection they are judged based on a  $R_{DS(on)}$ ,  $Q_G$ , thermal and dissipation properties. To speed up this process, a Matlab program was developed. The code to this script can be found in Appendix A. This program contains all variables relevant to our boost-converter system. It reads the MOSFET parameters and calculates all the equations presented in chapter 4. Some devices failed to meet the thermal requirements, such as operating in a 60 °C ambient temperature, where others presented too high  $R_{DS(on)}$  etcetera. From all possible options, three devices came out as best options, they are summarized in 5.3.

Table 5.3: MOSFET Selection [46, 47, 48]

No heatsinks, $T_A = 60^\circ\text{C}$							
Device	$R_{DS(on)}$ ( $m\Omega$ )	$Q_G$ (nC)	$\theta_{JA}$ ( $^\circ\text{C}/\text{W}$ )	$P_{cond}$ (W)	$P_{SW}$ (W)	$P_{Diss}$ (W)	$\Delta T_{JA}$ ( $^\circ\text{C}$ )
STF20NF20	100	28	62.5	0.84	1.21	2.10	> 115
IRFSL4620	63.7	25	40	0.78	0.64	1.42	56.9
IRFU220N	600	15	110	7.25	0.48	7.73	> 115
With heatsink, $T_A = 60^\circ\text{C}$ , $\theta_{HA} = 8.97(^\circ\text{C}/\text{W})$							
Device	$R_{DS(on)}$ ( $m\Omega$ )	$Q_G$ (nC)	$\theta_{JA}$ ( $^\circ\text{C}/\text{W}$ )	$P_{cond}$ (W)	$P_{SW}$ (W)	$P_{Diss}$ (W)	$\Delta T_{JA}$ ( $^\circ\text{C}$ )
STF20NF20	100	28	15.0	0.84	0.90	1.74	26.1
IRFSL4620	63.7	25	11	0.55	0.78	1.33	14.6
IRFU220N	600	15	13.5	6.48	0.48	6.93	76.3

Table 5.3 has been calculated using worst-case scenario's and with standard heatsinks. Greyed out cells indicate that the  $T_J$  would rise above  $T_{J(max)}$ , destroying the device. We see that heatsinking of the MOSFETs will be necessary. This keeps the losses lower, a simple aluminium heatsink,  $\theta_{HA} = 8.97(^\circ\text{C}/\text{W})$ , has been chosen that fits the MOSFET packages. Based on these calculations, the device with the lowest losses,  $P_{Diss}$  could have been chosen. Because the MOSFET needs to be carefully matched to the driver, the final choice can only be made after the losses in the driver have been evaluated.

### 5.3 Gate driver

With the choice for the Power MOSFET narrowed down to the three options in table 5.3, the driver can be chosen.

**Gate-Source voltage** The first decision that has to be made is the gate drive voltage,  $V_{GS}$ . This is of importance as equation 4.16 shows that the dissipated power in the driver increases with  $V_{GS}^2$ . On the MOSFET side, a higher  $V_{GS}$  leads to a lower  $R_{DS(on)}$  and thus lower losses. However, it also creates a higher  $Q_G$  [49], thus leading to even higher driver losses. Lastly, a low  $V_{GS}$  limits the maximum drain current  $I_D$ . The choice for  $V_{GS}$  is therefore a typical engineering trade-off. For all the MOSFETs in table 5.3, a  $V_{GS}$  above 8V does not limit the  $I_D$ . With a minimum of 8V there are also no problems with the turn-on threshold voltage  $V_{TH}$ . For these MOSFETs



the  $R_{DS(on)}$  does not decrease significantly for a  $V_{GS}$  above roughly 10V [49, 50]. Unfortunately the manufacturers do not provide exact figures for this. Summarized in 5.4 are these figures for the different devices. For calculation of  $P_{Diss(driver)}$ , equation 4.16 has been used.

Table 5.4:  $V_{GS}$  Selection [46, 47, 48]

$f_{sw} = 100kHz, T_J = 25^\circ C$			
$V_{GS}$ (V)	$R_{DS(on)}$ (m $\Omega$ )	$Q_G$ (nC)	$P_{Diss(driver)}$ (W)
STF20NF20			
8	<i>n/a</i>	25	0.020
10	100	28	0.028
12	<i>n/a</i>	32.5	0.039
IRFSL4620			
8	<i>n/a</i>	18	0.014
10	63.7	23	0.023
12	<i>n/a</i>	27.5	0.033
IRFU220N			
8	<i>n/a</i>	10	0.010
10	600	15	0.015
12	<i>n/a</i>	17	0.021

Based on these figures, a  $V_{GS}$  of 10V has been chosen, as a trade-off between losses in the driver and the MOSFET.

**$I_{peak}$  and  $R_{driver}$**  As we have seen in chapter 4, the process of driver selection continues with the peak driver current. With equation 4.17 the assumed constant charge current is calculated for the devices. The gate charge time,  $t_{charge}$  is set at  $\frac{1}{100}$  of a single period of the switching frequency [50]:

$$t_{charge} = \frac{1}{100} * \frac{1}{f_{sw}} \quad (5.14)$$

Which, for  $f_{sw} = 100kHz$  is 100ns. The rule of thumb is to choose a driver with at least twice the calculated  $I_{charge}$  as its peak value. Table 5.5 summarizes the results.

Table 5.5: Driver peak current selection [46, 47, 48]

$f_{sw} = 100kHz, t_{charge} = 100ns, V_{GS} = 10V$			
Device	$Q_G$ (nC)	$I_{charge}$ (A)	$I_{peak}$ (A)
STF20NF20	28	0.28	0.56
IRFSL4620	23	0.23	0.46
IRFU220N	15	0.15	0.30

The second requirement on the driver was based on the maximum driver output resistance,  $R_{driver}$  (equation 4.18). This method requires a time constant  $TC$  to be set. With a  $V_{GS}$  of 10V, a  $TC$  of 1 means that the gate charge would be charged up to 6.3V. All MOSFETs are already fully turned on at this point, but for a safety margin a  $TC$  of 2 has been chosen.

Table 5.6: Driver  $R_{driver}$  selection [46, 47, 48]

$f_{sw} = 100kHz, t_{charge} = 100ns, V_{GS} = 10V, TC = 2$			
Device	$C_G$ (nF)	$R_{gate}$ ( $\Omega$ )	$R_{driver(max)}$ ( $\Omega$ )
STF20NF20	2.8	<i>n/a</i>	15.1
IRFSL4620	2.3	2.6	19.1
IRFU220N	1.5	<i>n/a</i>	30.7

Table 5.6 shows the results. For the STF20NF20 and IRFU220N, no  $R_{gate}$  is specified. The results, shown in gray, are based on an assumed value of  $R_{gate}$ , equal to that of the IRFSL4620. We see that the values are all quite high (above 15 $\Omega$ ), there will be no problems meeting this in a driver.

Like with the MOSFET, the Farnell database was used to select useful devices, based on rated output current, output resistance, availability and IC package. Based on these results a MIC4420 driver has been chosen. It provides a much higher current output than needed (6A peak), has low output resistance and drives the MOSFET gate to within a few mV of its  $V_{CC}$ . This means that a 10V supply to the MIC4420 is enough to provide the MOSFET with a  $V_{GS}$  of 10V. The calculated power dissipation in combination with each device is given in table 5.7. Equation 4.19 was used, which closely matches the values produced in table 5.4, especially at the higher  $T_A$ . Note that the output resistance is strongly dependent on the temperature. Worst case values have been given as well.

Table 5.7: Driver and MOSFET combination: Driver selection [46, 47, 48, 51]

$f_{sw} = 100kHz, V_{CC} = 10V, V_{GS} = 10V$		
MIC4420, $R_{OH} = 2.3 (\Omega), R_{OL} = 3.0 (\Omega), T_A = 25^\circ C$		
Device	$Q_G (nC)$	$P_{Diss(driver)} (W)$
STF20NF20	28	0.022
IRFSL4620	23	0.018
IRFU220N	15	0.012
MIC4420, $R_{OH} = 5.0 (\Omega), R_{OL} = 5.0 (\Omega), T_A = 125^\circ C$		
Device	$Q_G (nC)$	$P_{Diss(driver)} (W)$
STF20NF20	28	0.028
IRFSL4620	23	0.023
IRFU220N	15	0.015

**Summary** Choices for the MOSFET and driver have been presented and justified. We have seen that relative to the MOSFET, the power losses in the driver are small. For the combination of MOSFET and driver, typically only about 1.5% of the energy is dissipated in the driver. With the remaining 98.5% being dissipated in the MOSFET, it can easily be justified to choose the MOSFET with the lowest losses. From table 5.3 the lowest loss device is the IRFSL4620. In combination with the MIC4420 driver, the total losses amount to 1.36W. These are the devices that will be implemented in the prototype.

## Chapter 6

# Proof of concept

In this chapter, the proof of concept and the practical implementation of the total MPPT system. First, in section 6.1 an overview will be given how the proof of concept was built and what the overall complications were. Secondly, in section 6.2, 6.3, 6.4 a more specific description of the individual subsystems is given.

### 6.1 Implementation

To test the proof of concept, a breadboard was used for the sensors, gate driver and microcontroller. The reason for this is that it is easy to use and changes can be made very easily. However, there is a drawback: breadboards can only conduct 1A of current, which makes them unsuitable for the boost-converter part, which is rated up to 3.33A. For the boost-converter, a stripboard (Veroboard) was used because of the higher conduction capability. Unfortunately, this requires soldering which may cost some more time when changes need to be made.

In figure 6.1, the boost-converter, voltage and current sensor and the gate driver are shown. In table 6.2 the numbers are matched with their corresponding elements.

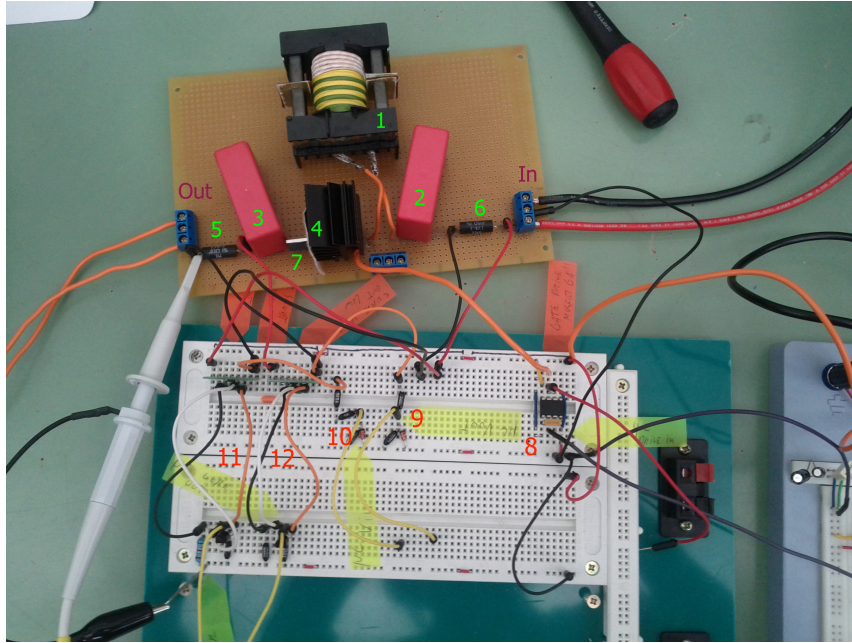


Figure 6.1: Proof of concept, practical implementation

Table 6.1: Practical implementation overview legend

#	Element	Value
1	Inductor	$112\mu H$
2	Input capacitor	$6.8\mu F$
3	Output capacitor	$6.8\mu F$
4	MOSFET with heatsink	-
5	Output shunt resistor	$0.03\Omega$
6	Input shunt resistor	$0.015\Omega$
7	Diode	-
8	Gate driver	MIC4420
9	Output voltage sensor	-
10	Input voltage sensor	-
11	Input current sensor	AD8212
12	Output current sensor	AD8212

## 6.2 Sensors

In this section, the practical sensor implementation will be discussed. First we will look at the current sensor and the difficulties implementing it, followed by the implementation of the voltage sensor.

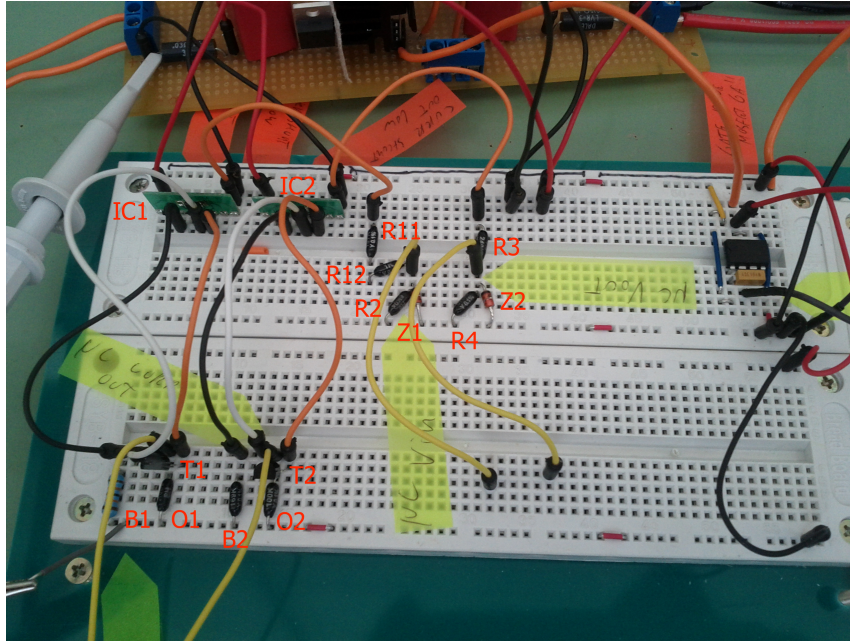


Figure 6.2: Practical implementation of the sensor modules

Table 6.2: Sensor implementation legend

#	Element	Value
IC1	Input current monitor	AD8212
IC2	Output current monitor	AD8212
T1,T2	PNP Transistor	BF423 / BC178
B1,B2	Bias resistors	In: $30k\Omega$ , Out: $170k\Omega$
O1, O2	Output resistors	In: $26.1k\Omega$ , Out: $33k\Omega$
R11, R12, R2	Input voltage sensor resistors	R11: $137k\Omega$ , R12: $1k\Omega$ , R2: $6k\Omega$
R3, R4	Output voltage sensor resistors	R3: $248k\Omega$ , R4: $8k\Omega$
Z1, Z2	Zener diodes	1N4733A

### 6.2.1 Current sensor

As described in chapter 5, for the current sensor the IC AD8212 was chosen for its accuracy and ease of implementation. The implementation of the current sensor using the AD8212 IC was straightforward. Following the scheme in chapter 5, the circuit was connected. A picture is shown in figure 6.2. The AD8212 is only available in MSOP (Minimal Small Outline Package), which cannot be inserted into the breadboard directly. The IC was soldered to an DIP (Dual In-line Package) which can easily be inserted into the breadboard.

### 6.2.2 Voltage sensor

In chapter 5, a design implementation for the voltage sensor was chosen. Due to simplicity, accuracy and ease of use, the voltage divider was chosen as most suitable option. The practical implementation is shown in figure 6.2. The design is not comprehensive, just two resistors in series, with a zener diode parallel to R2 and R4 for the input and output sensors, respectively.

## 6.3 Switching element

The IRFSL4620 MOSFET was chosen as the preferred device, however in order to compare its performance, the two other MOSFETS that were considered have been tested as well. This 'luxury' is possible because of the relative low cost of MOSFETS when compared to other components. The MOSFET is not mounted directly to the prototype board, but rather mounted in a socket. This allows for easy replacement in case of a failure, but also allows swapping one type of MOSFET with another quickly. Each MOSFET has been equipped with a clip-on heatsink, selected in chapter 6.

## 6.4 Gate driver

The gate driver MIC4420 was implemented in the prototype. figure 6.3 shows the setup, table 6.3 shows the numbered parts.

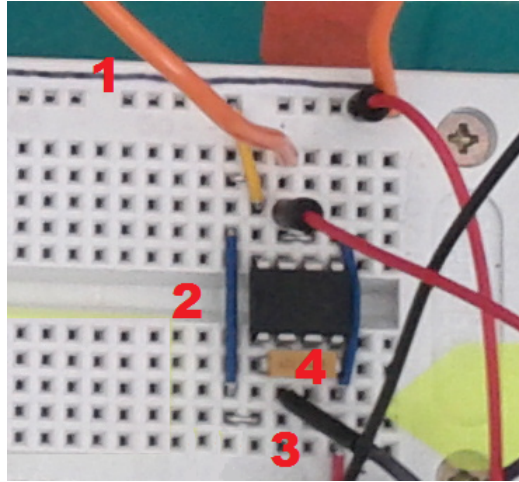


Figure 6.3: Implementation of the gate driver

Table 6.3: Driver overview legend

#	Element	Value
1	MOSFET gate connection	-
2	Supply voltage	0 – 12V
3	$\mu$ C PWM signal	-
4	Decoupling capacitor	100nF

After installation of the driver, testing could begin. It soon became apparent that there were some problems with the input signal from the microcontroller, which was corrupted with noise due to the length of the cable. Re-routing the cable solved this. Next, measurements on the output revealed large oscillations on the switching waveforms. It is suspected that this is due to interactions between the MOSFET gate capacitance  $C_G$ , the driver capacitance  $C_D$  and the drive wire inductance  $L_w$ . Decreasing the drive wire length was not an option since the MOSFET could not be placed closer to the driver. Placing the driver on the stripboard close to the driver was problematic, since a MOSFET failure also destroys the driver. This would mean that each time a MOSFET fails a lot of soldering has to be done on the driver and its peripherals. In order to damp the oscillations, a small external resistor of  $5\Omega$  was installed between the driver output and the MOSFET gate. A disadvantage of this resistor is that it creates a RC time, which causes the current flowing into the gate to be delayed, which



will cause the MOSFET to switch slower. Figure 6.4 shows the results. The white waveform (snapshot) shows the switching waveform without the external resistor, the coloured lines represent the situation with the  $5\Omega$  resistor.

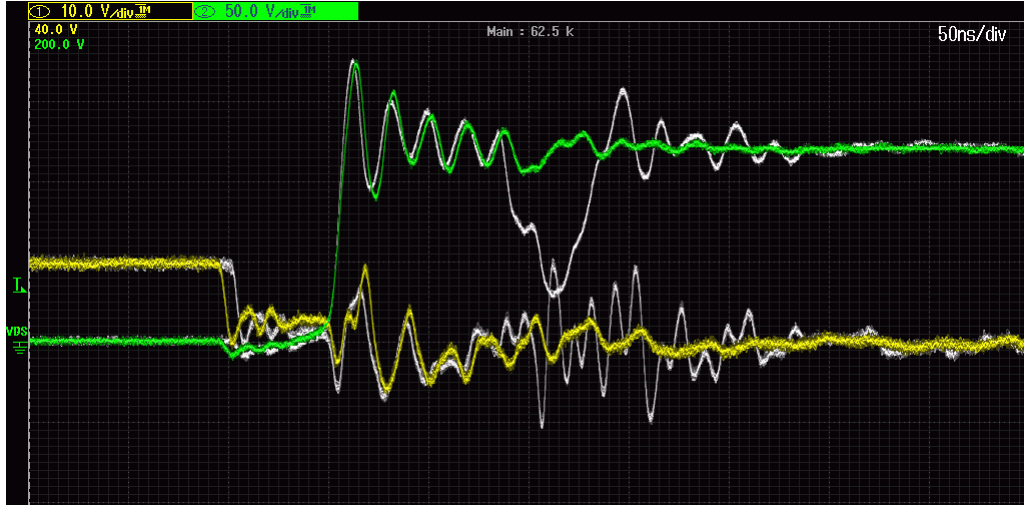


Figure 6.4: Gate drive and drain-source voltage waveform with STF20NF20 with (coloured) and without (white) external  $5\Omega$  resistor.

We see that the oscillations in  $V_{GS}$  have been damped to a large extent, where also the  $V_{DS}$  reaches its final value quicker and is generally much more stable.

# Chapter 7

## Evaluation

In this chapter, the proof of concept, described in chapter 6 will be evaluated. Evaluation is done by use of measurements. In section 7.1, the efficiency of the MPPT with different MOSFETs is evaluated. Followed by an evaluation of the gate switching behaviour in section 7.2. Lastly the power consumption of the control circuitry will briefly be discussed in section 7.4. This chapter is ended with a summary of the evaluations.

### 7.1 Efficiency Measurements

The efficiency measurements were done with the three selected MOSFETs of chapter 5. For each MOSFET, measurements were done at different duty cycles of the gate driver and different voltages at the input. In figures 7.1, 7.2, ??, for the IRFSL4620, STF20NF20 and IRFU220NBPF, respectively, the efficiency measured at different values of the duty cycle are plotted against the input power.

During testing, the input voltage was varied between 50V and 120V. First, we used a 0 – 70V power supply with a maximum current of 22A. In order to take measurements above 70V a 0 – 600V supply that is current limited to 2.6A, was used. Due to the 2.6A input current limit, some measurements in the 70 – 120V range could not be performed. All measurement data from the IRFSL4620 can be found in Appendix D.

**IRFSL4620** Figure 7.1 shows that the efficiency improves at higher input power. Also, the efficiency seems to be linear increasing with increasing input power. The 40% duty-cycle measurement seems to diverge a bit from its linear behaviour, this is probably due to inaccurate measurements. This

is in-line with the expectations.

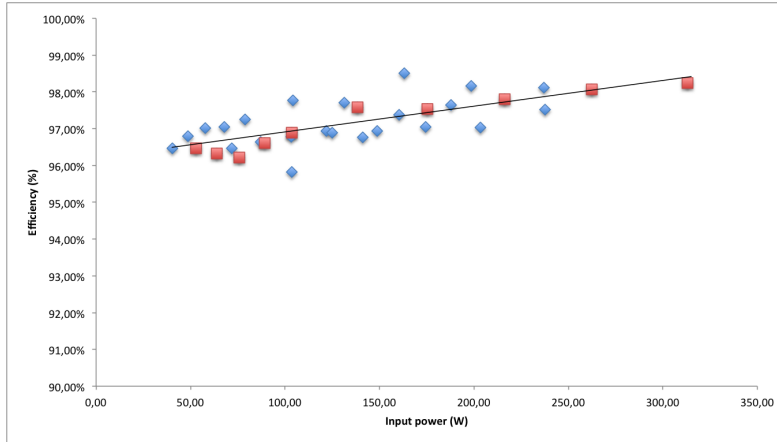


Figure 7.1: Efficiency vs. Input power at different duty-cycles IRFSL4620, 100Ω load

**STF20NF20** In figure 7.2, the efficiency of the second MOSFET is plotted against the input power. What can be seen is that the efficiency is again linear with the input power, except for the case of 20% duty-cycle, where it seems to diverge. The overall efficiency of the STF20NF20 is lower than the IRFSL4620 until about 100W where it is the same. Again, this is in-line with our expectations.

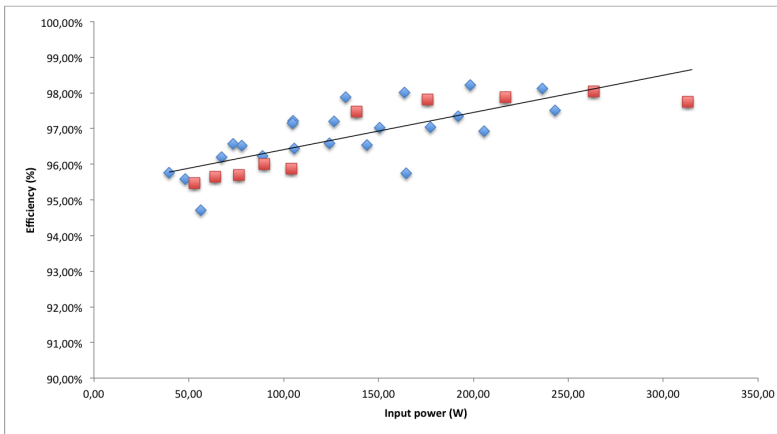


Figure 7.2: Efficiency vs. Input power at different duty-cycles STF20NF20, 100Ω load

**IRFU220NBPF** The efficiency of the IRFU220NBPF seems linear with the input power. However, at a duty cycle  $> 50\%$  the efficiency seems to decrease and the MOSFET fails. During testing, two MOSFETs of this type were destroyed. This was somewhat unexpected. Expectations were that the MOSFET would last longer.

## 7.2 Gate driving

This section will describe the results that were obtained by measuring the gate voltage  $V_{gs}$  (shown in yellow) and the drain-to-source voltage  $V_{ds}$  (shown in green). The measurements that are shown in this section are all done with an external  $R_{gate}$  resistor, which had a value of  $5\Omega$ . First the results of the IRFSL4620 will be presented, followed by the STF20NF20 and last the IRFU220NPBF.

**IRFSL4620** In figure 7.3, the  $V_{gs}$  and the  $V_{ds}$  are shown.  $V_{gs}$  the voltage of the gate driver increases to  $10V$  in about  $\frac{1}{50}ns$  and then drops, because of the gate capacitance ( $C_g$ ). This oscillation is constant with a period of  $\frac{2.5}{50}ns$ . When  $V_{gs}$  reaches its third peak,  $V_{ds}$  drops rapidly in about  $20ns$ , where after it remains fairly constant at  $0V$ .  $V_{gs}$  keeps oscillating heavily from  $5 - 17V$  at first but damps after  $200ns$  to about  $9 - 11V$ . Table 7.1 shows the measured values and the specified datasheet values. The datasheet values have been specified at different parameter ( $V_{DS}$ ,  $I_D$ ,  $R_{gate}$ ) values, and this table allows us to compare the timing delays of the MOSFET under different operating conditions.

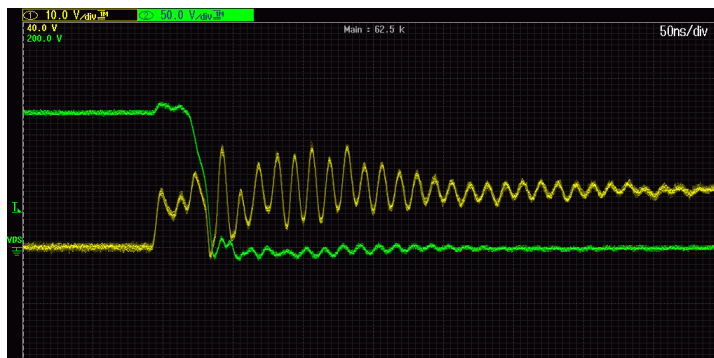


Figure 7.3: Turn-on of IRFSL4620,  $V_{gs} = 10V$ ,  $V_{in} = 60V$ ,  $R_{gate} = 5\Omega$

Table 7.1: Measured quantities IRFSL4620

Parameter	Measured (ns)	Datasheet (ns) [47]
Turn on delay time	25	13, 4
Rise time	15	22, 4
Turn off delay time	40	25, 4
Fall time	10	14, 8

Turn-off is shown in figure 7.4. At first,  $V_{gs}$  is stable at  $10V$ . When the  $V_{gs}$  drops to  $0V$  the  $V_{ds}$  response is delayed by  $45ns$ , where after the  $V_{ds}$  increases to  $V_{in}$  in  $10ns$ . After  $V_{ds}$  rose and  $V_{gs}$  fell, there is some transient behaviour, which damps out after about  $250ns$ .

Figure 7.4: Turn-off of IRFSL4620,  $V_{gs} = 10V$ ,  $V_{in} = 60V$ ,  $R_{gate} = 5\Omega$ 

**STF20NF20** Similar switching behaviour when compared to the IRFSL4620 can be seen with the STF20NF20 MOSFET (shown in figure 7.5). As with the previous MOSFET, the voltage of the gate driver increases for in about  $\frac{1}{50}ns$  to the intended  $10V$  then drops, because of the gate capacitance ( $C_g$ ).  $V_{ds}$  decreases in  $25ns$  to  $0V$  where it remains fairly constant.  $V_{gs}$  on the other hands remains oscillating heavily between  $3 - 17V$  for about  $45ns$ , after which it remains reasonably stable.



Figure 7.5: Turn-on of STF20NF20,  $V_{gs} = 10V$ ,  $V_{in} = 60V$ ,  $R_{gate} = 5\Omega$

Table 7.2: Measured quantities STF20NF20

Parameter	Measured (ns)	Datasheet (ns) [46]
Turn on delay time	15	15
Rise time	15	30
Turn off delay time	50	40
Fall time	10	10

The off switching behaviour is different from the IRFSL4620.  $V_{gs}$  damps much slower than the previous MOSFET, in about  $50ns$ . We also see in figure 7.6 that the MOSFET is turned on again when it is not supposed to. This is due to oscillations in the drive voltage rising above the threshold. Table 7.2 again shows the timing values. Here we see that the timings more closely match the specified values in the datasheet, despite differing operating conditions.

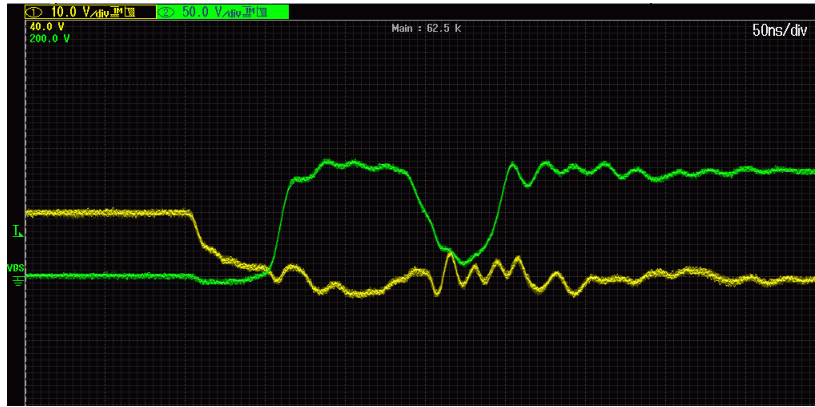


Figure 7.6: Turn-off of STF20NF20,  $V_{gs} = 10V$ ,  $V_{in} = 60V$ ,  $R_{gate} = 5\Omega$

**IRFU220** Compared to the other MOSFETs, we see that the IRFU220 has the 'nicest' switching behaviour, with the least delay times and relative small oscillations. Table 7.3 shows the timing signals. We see that the specified values closely match the measured values. The specified timing values for this MOSFET are generally much lower than both other devices, a result of the low ( $15nC$ ) gate charge. Unfortunately, this MOSFET comes in a relative small I-Pak package and we had problems fitting it to the heatsinks. Although test results were somewhat promising for this MOSFET, the cooling problems led to a few destroyed devices.

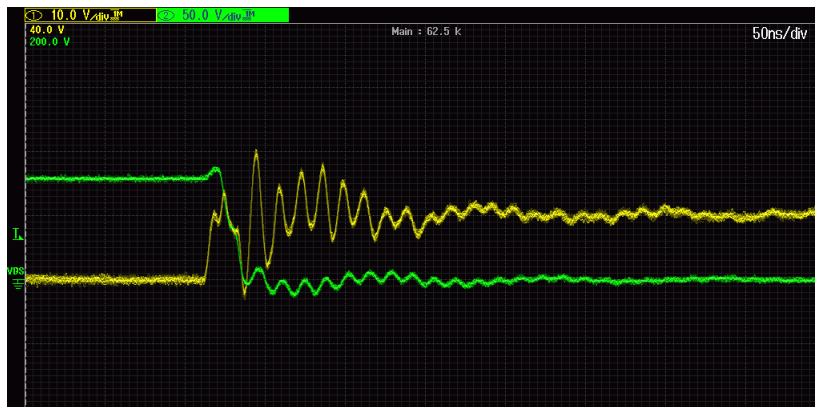
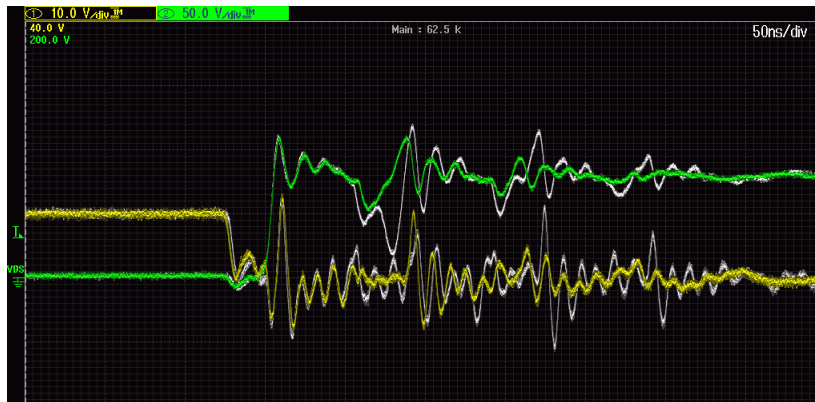


Figure 7.7: Turn-on of IRFU220,  $V_{gs} = 10V$ ,  $V_{in} = 40V$ ,  $R_{gate} = 5\Omega$

Table 7.3: Measured quantities IRFU220

Parameter	Measured (ns)	Datasheet (ns) [48]
Turn on delay time	10	6, 4
Rise time	10	11
Turn off delay time	25	20
Fall time	8	12

Figure 7.8: Turn-off of IRFU220,  $V_{gs} = 10V$ ,  $V_{in} = 40V$ ,  $R_{gate} = 5\Omega$ 

### 7.3 Sensors

The current and voltage sensors, designed in chapter 5 were tested. The voltage sensor, which consists of a simple voltage divider acted almost as expected. However, the Zener diode decreased the accuracy significantly. The Zener diodes were removed.

The current sensor caused more problems. The chosen transistor in chapter 5 (the BF423) was replaced by a different PNP transistor (BC178), because it did not go into conduction mode. Apart from this problem, the current sensor is very noisy. This is due to the very small signal, which is in the order of a few  $100mV$ . This can be solved by using shielded lines for the current sensors' input.



## 7.4 Control circuitry

The gate is driven by the MIC4420 driver chip. This driver is in turn controlled by the PWM signal from the ATmega 168 microcontroller [33]. In chapter 5 we calculated that the power dissipation of the driver would be  $0.023W$  for this setup. The proof-of-concept is connected to a  $10V$  voltage supply. The ATmega requires  $5V$ , which for practical reasons is provided by a Low Drop Output (LDO) regulator. The total dissipation of the driver, LDO and microcontroller combined has been measured at  $0.3W$ . With the LDO dissipating  $0.15W$  and the ATmega  $0.1W$ , we arrive at a measured dissipation of  $0.05W$  for the gate driver. This is higher than calculated, however this could be attributed to inaccurate measurements. Although the total dissipation of the control circuit is small compared to that of the converter, some improvement could be made by replacing the LDO with a more efficient  $10V$  to  $5V$  DC-DC converter. This is however beyond the scope of this thesis.

**Summary** We have measured the efficiency of the DC-DC converter and looked at the MOSFET behaviour in this system. Converter efficiencies for all devices was found to be  $> 95\%$  under almost all circumstances. It was shown that the device chosen in chapter 5, the IRFSL4620, indeed is the most efficient MOSFET of the three tested devices. All three MOSFETs meet the set requirements when it comes to timing and other requirements. The IRFU220 was not tested successfully at some duty cycles due to device failures, however a better cooling solution could fix this. This has not been done since calculations already showed that this device will be less efficient. Thermal properties of the MOSFETs under load have not been measured. Thermal performance could be evaluated by measuring heatsink temperatures (thermocouple or non-contact measurements using infrared) and comparing them to our design values. These measurements have not been implemented due to lack of time. Since both the IRFSL4620 and STF20NF2 have operated under full load for long times ( $> 15$  minutes) without failure or excessive heat production, we assume that the proposed heatsink functions properly.

## Chapter 8

# Conclusion & Recommendations

In this thesis a distributed maximum power point tracking system for use in the Nuna 6 solar racing vehicle was proposed. The advantages of this system under changing lighting conditions were shown with Simulink simulations. As a part of this proposed system, a DC-DC boost converter proof-of-concept has been built. For the boost converter, this thesis describes the design process of the switching element, gate driver and sensors. The proof-of-concept boost converter has been tested and proved to be 97.1% efficient at the specified operating conditions. This is a typical value for this type of power electronics. This value exceeds our requirements.

In cooperation with the two other theses belonging to this project, the principle of distributed tracking and the proof-of-concept of this system have been shown to function properly. However, this is only a first step in the process of developing a prototype that can be tested and eventually used under race conditions. To create a practical system of multiple trackers, further study into the optimal distributed tracking architecture (primarily the number of trackers for maximum power output) is required. On the boost converter module, more effort could be put into finding more efficient boost converter topologies and advanced soft-switching techniques to further decrease converter losses. To design a reliable product for use in the actual vehicle, we recommend further study into making an off-the-shelf reliable, safe, robust and user-friendly product. Which meets all specific considerations and requirements regarding the Nuna or other solar racing vehicles.

# Bibliography

- [1] G. I. A. V. B. Omubo-Pepple, C. Israel-Cookey, “Effects of temperature, solar flux and relative humidity on the efficient conversion of solar energy to electricity,” *European Journal of Scientific Research*, vol. 35, no. 2, pp. 173–180, 2009.
- [2] M. Patel, *Wind and Solar Power Systems: Design, Analysis, and Operation*, ser. Mechanical Engineering. Taylor & Francis, 2006. [Online]. Available: <http://books.google.nl/books?id=8aQDw14fQnkC>
- [3] C.-C. Chu and C.-L. Chen, “Robust maximum power point tracking method for photovoltaic cells: A sliding mode control approach,” *Solar Energy*, vol. 83, no. 8, pp. 1370 – 1378, 2009. [Online]. Available: <http://www.sciencedirect.com/science/article/pii/S0038092X09000516>
- [4] R. Giral, C. Carrejo, M. Vermeersh, A. Saavedra-Montes, and C. Ramos-Paja, “Pv field distributed maximum power point tracking by means of an active bypass converter,” in *Clean Electrical Power (ICCEP), 2011 International Conference on*, june 2011, pp. 94 –98.
- [5] N. Femia, G. Lisi, G. Petrone, G. Spagnuolo, and M. Vitelli, “Distributed maximum power point tracking of photovoltaic arrays: Novel approach and system analysis,” *Industrial Electronics, IEEE Transactions on*, vol. 55, no. 7, pp. 2610 –2621, july 2008.
- [6] S. Poshtkouhi, V. Palaniappan, M. Fard, and O. Trescases, “A general approach for quantifying the benefit of distributed power electronics for fine grained mppt in photovoltaic applications using 3d modeling,” *Power Electronics, IEEE Transactions on*, vol. PP, no. 99, p. 1, 2011.
- [7] M. K. Kazimierczuk, *Pulse-width Modulated DC-DC Power Converters*. Wiley, 2008.

- [8] M. D. Seeman, “Analytical and practical analysis of switched-capacitor dc-dc converters,” Ph.D. dissertation, 2006.
- [9] L. Pylarinos, “Charge pumps: An overview,” in *Proceedings of the IEEE International Symposium on Circuits and Systems*, 2003.
- [10] G. Palumbo and D. Pappalardo, “Charge pump circuits: An overview on design strategies and topologies,” *Circuits and Systems Magazine, IEEE*, vol. 10, no. 1, pp. 31–45, 2010.
- [11] G. Hua and F. C. Lee, “Soft-switching pwm techniques and their applications,” in *Power Electronics and Applications, 1993., Fifth European Conference on*, pp. 87–92 vol.3.
- [12] C. P. Basso, *Switch-Mode Power Supplies: SPICE Simulations and Practical Designs*. McGraw-Hill, 2008.
- [13] K. H. Liu and F. C. Y. Lee, “Zero-voltage switching technique in dc/dc converters,” *Power Electronics, IEEE Transactions on*, vol. 5, no. 3, pp. 293–304, 1990.
- [14] M. Bildgen, *Resonant converter topologies*. ST Microelectronics, 1999. [Online]. Available: <http://www.datasheetcatalog.org/datasheet/SGSThompsonMicroelectronics/mXyzxvt.pdf>
- [15] J. Bauman and M. Kazerani, “A novel capacitor-switched regenerative snubber for dc/dc boost converters,” *Industrial Electronics, IEEE Transactions on*, vol. 58, no. 2, pp. 514–523, 2011.
- [16] J. Marshall and M. Kazerani, “A novel lossless snubber for boost converters,” in *Industrial Electronics, 2006 IEEE International Symposium on*, vol. 2, pp. 1030–1035.
- [17] J. Smith, K. M. and K. M. Smedley, “Properties and synthesis of passive lossless soft-switching pwm converters,” *Power Electronics, IEEE Transactions on*, vol. 14, no. 5, pp. 890–899, 1999.
- [18] Y. Konishi and H. Yung-Fu, “Soft-switching buck boost converter using passive snubber composed of pulse current regenerative resonant circuit,” in *Telecommunications Energy Conference, 2007. INTELEC 2007. 29th International*, pp. 886–890.
- [19] P. Bode, “Application note 39 current measurement applications handbook,” 2008. [Online]. Available: [http://www.diodes.com/\\_files/products.appnote.pdfs/zetex/an39.pdf](http://www.diodes.com/_files/products.appnote.pdfs/zetex/an39.pdf)

- [20] Keithley, *Low level measurements handbook, precision dc current, voltage and resistance measurements*. Keithley, 2004.
- [21] N. Pilling, R. Holmes, and G. Jones, “Low-power optical current measurement system employing a hybrid transmitter,” *Science, Measurement and Technology, IEE Proceedings -*, vol. 141, no. 2, pp. 129–134, mar 1994.
- [22] J. Webster, *The Measurement, Instrumentation, and Sensors Handbook*, ser. Electrical Engineering Handbook Series. CRC Press, 1999. [Online]. Available: <http://books.google.nl/books?id=b7UuZzf9ivIC>
- [23] C. Blake and C. Bull, “Igbt or mosfet: Choose wisely.” [Online]. Available: [www.irf.com/technical-info/whitepaper/choosewisely.pdf](http://www.irf.com/technical-info/whitepaper/choosewisely.pdf)
- [24] W. Konrong, F. C. Lee, H. Guichao, and D. Borojevic, “A comparative study of switching losses of igbts under hard-switching, zero-voltage-switching and zero-current-switching,” in *Power Electronics Specialists Conference, PESC '94 Record., 25th Annual IEEE*, pp. 1196–1204 vol.2.
- [25] Powerex, “Cm150du-12f datasheet.” [Online]. Available: <http://pdf1.alldatasheet.com/datasheet-pdf/view/20687/POWEREX/CM150DU-12F.html>
- [26] International Rectifier, “Power mosfet basics,” 2001. [Online]. Available: [www.irf.com/technical-info/appnotes/mosfet.pdf](http://www.irf.com/technical-info/appnotes/mosfet.pdf)
- [27] N. Mohan, T. M. Undeland, and W. P. Robbins, “Power electronics - converters, applications, and design (3rd edition),” 2003.
- [28] International Rectifier, “Application note an-937: Gate drive characteristics an requirements for hexfet power mosfets.” [Online]. Available: [www.irf.com/technical-info/appnotes/an-937.pdf](http://www.irf.com/technical-info/appnotes/an-937.pdf)
- [29] Microchip Technology, “Application note an898 determining mosfet driver needs for motor drive applications,” 2003. [Online]. Available: <http://ww1.microchip.com/downloads/en/AppNotes/00898a.pdf>
- [30] H. Rashid, *Power Electronics Handbook: Devices, Circuits, and Applications*. Elsevier, 2010.
- [31] CLARE, “Mosfet/igbt drivers application note an-401,” 2012. [Online]. Available: [pdfserv.maxim-ic.com/en/an/AN401.pdf](http://pdfserv.maxim-ic.com/en/an/AN401.pdf)

- [32] A. T. Sluimer and F. Nassiri Nia, “Converter design for maximum power point tracking,” To be published.
- [33] S. Moring and A. F. Pols, “Maximum power point tracking: Algorithm and software development,” To be published.
- [34] Panasonic, “NNP Series NCR18650A Datasheet,” 2009. [Online]. Available: <http://industrial.panasonic.com/www-data/pdf/ACA4000/ACA4000PE6.pdf>
- [35] Panasonic, “Lithium Ion Batteries Technical Handbook,” 2007. [Online]. Available: [http://industrial.panasonic.com/www-ctlg/ctlg/qACI4000\\_EU.html](http://industrial.panasonic.com/www-ctlg/ctlg/qACI4000_EU.html)
- [36] Wikipedia, “Boost converter topology,” may 2012. [Online]. Available: [http://upload.wikimedia.org/wikipedia/en/9/9f/Boost\\_circuit.png](http://upload.wikimedia.org/wikipedia/en/9/9f/Boost_circuit.png)
- [37] D. M. Robert Warren Erickson, *Fundamentals of Power Electronics*. Springer, 2001.
- [38] I. Budihardjo and P. G. Lauritzen, “The lumped-charge power mosfet model, including parameter extraction,” *Power Electronics, IEEE Transactions on*, vol. 10, no. 3, pp. 379–387, 1995.
- [39] International Rectifier, “Application note an-944: Use gate charge to design the gate drive circuit for power mosfets and igbts.” [Online]. Available: [www.irf.com/technical-info/appnotes/an-944.pdf](http://www.irf.com/technical-info/appnotes/an-944.pdf)
- [40] G. Dusan, M. Purschnel, and A. Kiep, “Infineon mosfet power losses calculation using the data-sheet parameters.” [Online]. Available: [http://www.btipnow.com/library/white\\_papers/MOSFETPowerLossesCalculationUsingtheData-SheetParameters.pdf](http://www.btipnow.com/library/white_papers/MOSFETPowerLossesCalculationUsingtheData-SheetParameters.pdf)
- [41] MAXIM, “Application note 1832: Power supply engineer’s guide to calculate dissipation for mosfets in high-power supplies,” 2002. [Online]. Available: <http://pdfserv.maxim-ic.com/en/an/AN1832.pdf>
- [42] Electus, “Application note: Heatsink basics.” [Online]. Available: [http://www.electusdistribution.com.au/images\\_uploaded/heatsink.pdf](http://www.electusdistribution.com.au/images_uploaded/heatsink.pdf)
- [43] MAXIM, “Application note 746: High-side current sense measurement: Circuits and principles,” 2001. [Online]. Available: <http://pdfserv.maxim-ic.com/en/an/AN746.pdf>

- [44] Supertex Inc., “Hv7801 datasheet,” 2008. [Online]. Available: [www.supertex.com/pdf/datasheets/HV7801.pdf](http://www.supertex.com/pdf/datasheets/HV7801.pdf)
- [45] Analog Devices, “AD8212 Datasheet,” 2009. [Online]. Available: [www.analog.com/static/imported.../AD8212.pdf](http://www.analog.com/static/imported.../AD8212.pdf)
- [46] STMicroelectronics, “STD20NF20/STF20NF20/STP20NF20 Datasheet,” 2009. [Online]. Available: [http://www.st.com/internet/com/technical\\_resources/technical\\_literature/datasheet/CD00150587.pdf](http://www.st.com/internet/com/technical_resources/technical_literature/datasheet/CD00150587.pdf)
- [47] International Rectifier, “IRFS4620PbF/IRFSL4620PbF Datasheet,” 2008. [Online]. Available: <http://www.irf.com/product-info/datasheets/data/irfs4620pbf.pdf>
- [48] International Rectifier, “IRFR220N/IRFU220N Datasheet,” 2000. [Online]. Available: <http://www.irf.com/product-info/datasheets/data/irfr220n.pdf>
- [49] Texas Instruments, “Application note: Optimizing mosfet gate drive voltage.” [Online]. Available: <http://www.ti.com/litv/pdf/slua341>
- [50] Microchip, “Application note an799: Matching mosfet drivers to mosfets,” 2004. [Online]. Available: <http://ww1.microchip.com/downloads/en/AppNotes/00799b.pdf>
- [51] MICREL, “Mic4420/4429 datasheet,” 2005. [Online]. Available: [www.micrel.com/\\_PDF/mic4420.pdf](http://www.micrel.com/_PDF/mic4420.pdf)

# Glossary

$\Delta T$	Temperature rise [°C]
$\theta$	Thermal resistance
<i>ADC</i>	Analogue-to-digital conversion
$V_{BR}$	Breakdown voltage [V]
$Q$	Charge [C]
$I_{charge}$	Charge current [A]
<i>CMRR</i>	Common mode rejection ratio
<i>CCM</i>	Continuous conduction mode
$I$	Current [A]
<i>DCM</i>	Discontinuous conduction mode
$I_d$	Drain current [A]
$V_{DS}$	Drain-source Voltage [V]
$R_{driver}$	Driver output resistance [ $\Omega$ ]
$R_{OH}$	Driver output resistance, high output [ $\Omega$ ]
$V_{DS}$	Drain-source Voltage [V]
$R_{driver}$	Driver output resistance [ $\Omega$ ]
$R_{OH}$	Driver output resistance, high output [ $\Omega$ ]
$R_{OL}$	Driver output resistance, low output [ $\Omega$ ]
<i>EMI</i>	Electromagnetic interference
<i>ESR</i>	Equivalent series resistance [ $\Omega$ ]
$f$	Frequency [Hz]
$C_G$	Gate capacitance [F]
$Q_G$	Gate charge [C]
$R_{gate}$	Gate resistance [ $\Omega$ ]
$C_{GD}$	Gate-drain capacitance ("Miller") [F]



$C_{GS}$	Gate-source capacitance [F]
$V_{GS}$	Gate-source voltage [V]
$I_L$	Inductor current [A]
$L_C$	Inductor-capacitor
<i>IGBT</i>	Insulated gate bipolar transistor
$T_j$	Junction Temperature [ $^{\circ}\text{C}$ ]
$R_L$	Load Resistance [ $\Omega$ ]
$I_M$	Maximum drain current [A]
<i>MPPT</i>	Maximum power point tracking
<i>MOSFET</i>	Metal-oxide-semiconductor field-effect transistor
$C_{iss}$	MOSFET input capacitance [F]
$R_{DS(on)}$	MOSFET on-state resistance [ $\Omega$ ]
$C_{oss}$	MOSFET output capacitance [F]
$C_{rss}$	MOSFET reverse transfer capacitance [F]
$V_{off}$	Off-state voltage [V]
$C_O$	Output capacitance [F]
$V_O$	Output voltage [V]
$I_{peak}$	Peak current rating [A]
<i>PV</i>	Photovoltaic
$P$	Power [W]
<i>PWM</i>	Pulse width modulation
<i>SOA</i>	Safe operating area
<i>SiC</i>	Silicon carbide
$f_{sw}$	Switching frequency [Hz]
<i>SMPS</i>	Switch-mode power supply
$T$	Time [s]
<i>TC</i>	Time constant
<i>ZCS</i>	Zero current switching
<i>ZVS</i>	Zero voltage switching

# List of Figures

2.1	Temperature dependency of a solar panel, source: [3]	4
2.2	Light intensity dependency of a solar panel, source: [3]	4
3.1	Classification of power supply technologies, source: [7]	8
3.2	Shunt current sensor, source: [20]	10
3.3	Voltage division	12
3.4	Preferred operating regions for MOSFET and IGBT, source: [23]	13
3.5	Preferred operating regions for MOSFET and BJT, source: [26]	13
4.1	Total system overview of the Nuna 6	16
4.2	Division of sensor submodule into functional elements	17
4.3	Division of boost converter submodule into functional elements	17
4.4	Division of controller submodule into functional elements	18
4.5	Partial solar panel model	19
4.6	DriveTek V4 Converter model	20
4.7	SolarMax Converter model	21
4.8	The complete combined model	23
4.9	Output power for equal insolation of $1000W/m^2$	23
4.10	Output power for insolation 1000 and $2000W/m^2$	24
4.11	Output power for insolation 750 and $1000W/m^2$	25
4.12	Voltage divider	28
4.13	Boost converter topology, source: [36]	29
4.14	MOSFET with junction capacitance, source: [30]	30
4.15	Variation of $C_{gd}$ and $C_{gs}$ as a function of $V_{DS}$ , source: [30]	31
4.16	Microchip T442X 9A MOSFET Driver, source: [29]	36
4.17	Microchip T442X charging external gate, source: [29]	36
5.1	AD8212 Topology, source: [45]	41
5.2	AD8212 Bias resistor chart, source: [45]	43

6.1	Proof of concept, practical implementation . . . . .	52
6.2	Practical implementation of the sensor modules . . . . .	53
6.3	Implementation of the gate driver . . . . .	55
6.4	Gate drive and drain-source voltage waveform with STF20NF20 with (coloured) and without (white) external $5\Omega$ resistor. . .	56
7.1	Efficiency vs. Input power at different duty-cycles IRFSL4620, $100\Omega$ load . . . . .	58
7.2	Efficiency vs. Input power at different duty-cycles STF20NF20, $100\Omega$ load . . . . .	58
7.3	Turn-on of IRFSL4620, $V_{gs} = 10V$ , $V_{in} = 60V$ , $R_{gate} = 5\Omega$ .	59
7.4	Turn-off of IRFSL4620, $V_{gs} = 10V$ , $V_{in} = 60V$ , $R_{gate} = 5\Omega$ .	60
7.5	Turn-on of STF20NF20, $V_{gs} = 10V$ , $V_{in} = 60V$ , $R_{gate} = 5\Omega$	61
7.6	Turn-off of STF20NF20, $V_{gs} = 10V$ , $V_{in} = 60V$ , $R_{gate} = 5\Omega$	62
7.7	Turn-on of IRFU220, $V_{gs} = 10V$ , $V_{in} = 40V$ , $R_{gate} = 5\Omega$ . .	62
7.8	Turn-off of IRFU220, $V_{gs} = 10V$ , $V_{in} = 40V$ , $R_{gate} = 5\Omega$ . .	63

# List of Tables

3.1	Common current measuring methods [19]	9
3.2	Common voltage measuring methods [22]	11
5.1	Current Sense IC overview	40
5.2	MOSFET Operating requirements	46
5.3	MOSFET Selection [46, 47, 48]	47
5.4	$V_{GS}$ Selection [46, 47, 48]	48
5.5	Driver peak current selection [46, 47, 48]	49
5.6	Driver $R_{driver}$ selection [46, 47, 48]	49
5.7	Driver and MOSFET combination: Driver selection [46, 47, 48, 51]	50
6.1	Practical implementation overview legend	52
6.2	Sensor implementation legend	53
6.3	Driver overview legend	55
7.1	Measured quantities IRFSL4620	60
7.2	Measured quantities STF20NF20	61
7.3	Measured quantities IRFU220	63

# Appendix A - MOSFET Calculator

```
close all;
clear all;
clc;

%MOSFET AND DRIVER CALCULATOR%%%
disp('BAP NUNA Mosfet & Driver calculator ')

V_DS = input('Maximum Drain-Source voltage:   Default 160[V]');
if (isempty(V_DS))
    V_DS = 160;
end

D = input('Duty cycle:           Default 0.62[ ](RANGE 0-1)');
if (isempty(D))
    D = 0.62;
end

fsw = 1e3*input('Switching frequency:   Default 100[kHz]');
if (isempty(fsw))
    fsw = 100000;
end

disp('MOSFET CALCULATOR [0] OR DRIVER CALCULATOR [1]')
sel = input('[0/1]');

%%%%%%%%%%%%%%%%%%%%%%%%%%%%%%%%%%%%%%%%%%%%%%%%%%%%%%%%%%%%%%%%%%%%%%%%MOSFET BEGIN%%%%%%%%%%%%%%%%%%%%%%%%%%%%%%%%%%%%%%%%%%%%%%%%%%%%%%%%%%%%%%%%%%%%%%%%
if(sel == 0)

disp('General parameters') %ask for input, assume defaults when nothing is input

P_in = input('Input power: Default 200[W]');
if (isempty(P_in))
```

```

    P_in = 200;
end

V_in = input('Minimum input voltage:   Default 60[V]');
if (isempty(V_in))
    V_in = 60;
end

T_Amax = input('Max allowed Ambient Temp in housing:   Default 60[C]');
if (isempty(T_Amax))
    T_Amax = 60;
end

disp('MOSFET parameters, Defaults IRFSL4620') % DEFAULTS FOR IRFSL4620PBF
TJ_max = 175

t_on = 1e-9*input('MOSFET rise time:   22.4e-9[ns]');
if (isempty(t_on))
    t_on = 22.4e-9;
end

t_off = 1e-9*input('MOSFET fall time:   14.8e-9[ns]');
if (isempty(t_off))
    t_off = 14.8e-9;
end

R_DSON_spec = input('On state DrainSource resistance, R_DS_ON:   63.7e-3[Ohm]');
if (isempty(R_DSON_spec))
    R_DSON_spec = 63.7e-3;
end

T_spec = input('Temperature at which R_DS_ON is specified:   25[C]');
if (isempty(T_spec))
    T_spec = 25;
end

HS =input('Heatsink [1/0]?');
HSEmpty = isempty(HS);
if(HSEmpty == 1)
    HS =0;
end

if(HS==0)
theta_JA = input('Total Junction-to-Ambient thermal resistance:
40[C/W]');
    if (isempty(theta_JA))
        theta_JA = 40;
    end
end

```

```

elseif (HS ==1)
    theta_JC = input('MOSFET Junction-to-case thermal resistance:
1.045[C/W]');
    if (isempty(theta_JC))
        theta_JC = 1.045;
    end

    theta_CS = input('Case-to-sink thermal resistance:    1[C/W]');
    if (isempty(theta_CS))
        theta_CS = 1;
    end

    theta_SA = input('Heatsink-to-ambient thermal resistance:    8.97[C/W]');
    if (isempty(theta_SA))
        theta_SA = 8.97; % Indian chief heatsink
    end

    theta_JA = theta_JC+theta_CS+theta_SA

end

TJ_hot = input('Guess Junction operating temp:          [C]');

while 1

    I_in = P_in/V_in;
    I_Drms = sqrt(D*(I_in)^2);
    R_DSON_HOT = R_DSON_spec*(1+0.005*(TJ_hot-T_spec));
    P_CM = R_DSON_HOT*I_Drms^2;
    P_SWM = 0.5*V_DS*I_Drms*fsw*(t_on+t_off);
    P_M = P_CM+P_SWM;

    TJ_rise = P_M * theta_JA;
    T_A = TJ_hot-TJ_rise;

    if T_A<T_Amax %Ambient smaller than T_Amax, thus mosfet will get too hot when T_Amax is

        if TJ_hot>TJ_max
            disp('error terror,. Mosfet too hot')
            break
        end
    end
end

```

```

        TJ_hot = TJ_hot+1;
    end

    TJ_hot

    if T_A>T_Amax
        disp('De benodigde Ambient Temperature ligt hoger dan die temperatuur in de casing')
        c = input('doorgaan [1/0]?');
        if (c == 1)
            TJ_hot = TJ_hot-input('hoeveel aftrekken van TJ_hot?')
        end
        if (c==0)
            disp('TJ_rise')
            TJ_rise
            break
        end
    end

end

end

disp('Total losses in MOSFET in W')
disp('Conduction:')
disp(P_CM)
disp('switching:')
disp(P_SWM)
disp('Totaal:')
disp(P_M)

end

%%%%%%%%%%%%%%%%%%%%%%%%%%%%%%%%%%%%%%%%%%%%%%%%%%%%%%%%%%%%%%%%%%%%%%%%MOSFET END%%%%%%%%%%%%%%%%%%%%%%%%%%%%%%%%%%%%%%%%%%%%%%%%%%%%%%%%%%%%%%%%%%%%%%%%

%%%%%%%%%%%%%%%%%%%%%%%%%%%%%%%%%%%%%%%%%%%%%%%%%%%%%%%%%%%%%%%%%%%%%%%%DRIVER BEGIN%%%%%%%%%%%%%%%%%%%%%%%%%%%%%%%%%%%%%%%%%%%%%%%%%%%%%%%%%%%%%%%%%%%%%%%%

if(sel ==1)
    disp('WELKOM BIJ DE DRIVER SELECTOR')

    V_GS = input('Gate Source Voltage:   Default 10[V]');
    if (isempty(V_GS))
        V_GS = 10;
    end

end

Q_G = 1e-9*input('Typical Gate Charge:   Default 15 [nC]');
if (isempty(Q_G))
    Q_G = 15e-9;
end

end

```



```

%%%% FIRST ORDER DISSIPATION%%
C_G = Q_G/V_GS;
P_DISS_DRIVER = C_G * V_GS^2*fsw

P_DISS_DRIVER2 = Q_G * V_GS*fsw

%%%%FIRST ORDER CHARGE TIME, PEAK CHARGE CURRENT%%

%%t_Charge is 1/100 of 1 switching cycle
t_charge = (1/fsw)*(1/100)

i_charge = Q_G/t_charge

%%%% REQ ON RDRIVER%%
R_gate = input('MOSFET Gate_resistance:  Default 2.6 [Ohm]');
if (isempty(R_gate))
    R_gate = 2.6;
end

TC = input('number of TCs to charge gate (1-3):  Default 2 []');
if (isempty(TC))
    TC = 2;
end

R_driver = (t_charge/(C_G*TC))-R_gate

%%Advanced loss calculation%%

disp('Advanced dissipation calculation')

R_OL = input('Driver output resistance @ output LOW:  Default 3 [ohm]');
if (isempty(R_OL))
    R_OL = 3;
end

R_OH = input('Driver output resistance @ output HIGH:  Default 2.3 [ohm]');
if (isempty(R_OH))
    R_OH = 2.3;
end

V_CC = input('Driver Suppyl voltage:  Default equal to V_GS: 10 [V]');
if (isempty(V_CC))
    V_CC = V_GS;
end

```

```
P_Dadv = ((R_OH*V_CC*Q_G*fsw)/(R_OL))
```

```
end
```

```
disp('Run script again? [1/0]');
```

```
restart = input('[1/0]');
```

```
if(restart == 0)
```

```
end
```

```
if(restart ==1)
```

```
    mosfet_calculator
```

```
end
```

# Appendix B - Model Plotter

```
close all;

kies = input('Model draaien [0], alleen plotten [1]');

if (kies == 0)

mdl = 'MPPT';
    load_system(mdl);
    sim(mdl);

end

%duty = max(duty-cycle.signals.values);
insolation1 = max(Insolation_1.signals.values);
insolation2 = max(Insolation_2.signals.values);

figure(1)

subplot(221)
plot(Pout_SolarMax.signals.values)
title('Pout SolarMax')

subplot(222)
plot(Pout_DriveTek.signals.values)
title('Pout DriveTek')

subplot(223)
plot(Eout_SolarMax.signals.values)
title('Eout SolarMax: Total harvested energy')

subplot(224)
plot(Eout_DriveTek.signals.values)
title('Eout DriveTek: Total harvested energy')
```

```
ha = axes('Position',[0 0 1 1], 'Xlim',[0 1], 'Ylim',[0
    1], 'Box','off', 'Visible','off', 'Units','normalized', 'clipping' , 'off');

text(0.5, 1, ['Insolation 1: ' num2str(insolation1) ', Insolation 2: ' num2str(insolation2)

figure(2)

subplot(211)
plot(Pout_SolarMax.signals.values)
title('Pout SolarMax')

subplot(212)
plot(Pout_DriveTek.signals.values)
title('Pout DriveTek')

kies2 = input('Alle data weggooien [1], data bewaren [0]')

if (kies2 == 1)
    clear all;
    clc;

end
clc;
```

# Appendix C - Brief of requirements

In this section, we will present a list of general requirements of the MPPT system. These specifications are typical requirements that a customer might have. The MPPT should:

- fit into the Nuna 6;
- always produce the maximum power output of a solar panel;
- communicate one-way with the solar car;
- communicate through the CAN bus protocol;
- be able to be used by anyone without knowledge of the system;
- indicate its status with LEDs
- consist of only one unit;
- be as efficient as possible;
- be easily replaceable.

These requirements are formulated in more detail in following subsections.

## **Use of the MPPT**

- [2.2.1.1] The MPPT will maximize the output power of a connected solar cell under all conditions specified in the Usage Characteristics.
- [2.2.1.2] The MPPT will be installed fivefold in the Nuna 6 solar racing vehicle, this will be called the system.

- [2.2.1.3] The system can be installed, removed and operated by any Nuon Solar team member, without requiring prior knowledge of its inner workings.
- [2.2.1.4] The MPPT provides plug-and-play connectivity.
- [2.2.1.5] Each MPPT has an external reset switch.
- [2.2.1.5] The system will communicate with the vehicle.
- [2.2.1.6] The MPPTs operating status can be visually inspected.
- [2.2.1.7] The system will be robust, stable and safe.
- [2.2.1.8] The system will be constructed as light and compact as possible.
- [2.2.1.9] The system can be easily integrated into Nuna 6 and its future successors.
- [2.2.1.10] Each MPPT will have a life expectancy under normal operating conditions of at least 3 years.
- [2.2.1.11] The MPPT is maintenance free during its expected lifetime.

#### **Ecological requirements**

- [2.2.2.1] The system wastes as little energy as possible.
- [2.2.2.2] The production process has minimal environmental impact.
- [2.2.2.3] All components are RoHS compliant.

#### **Technical requirements**

- [2.2.3.1] A total of 5 on board MPPTs will provide Nuna 6 with more power under equal conditions than the current power point tracking system.
- [2.2.3.2] A fault in one of the MPPTs will not lead to loss of power to Nuna 6, other than the power controlled by the faulty MPPT itself.
- [2.2.3.3] The MPPT accepts input voltages between 60V and 120V.
- [2.2.3.4] The MPPT connects to the Nuna 6 power bus, providing an output voltage between 110V and 160V.

- [2.2.3.5] Should the output voltage rise above 160V, indicating a full battery on the Nuna vehicle, the system will stop tracking to prevent over-charging.
- [2.2.3.6] The systems nominal input power is between 20W and 100W with an absolute maximum of 200W.
- [2.2.3.7] The average efficiency of each MPPT will be greater than 95%.
- [2.2.3.8] The system operates without malfunction with environmental temperatures ranging between  $-10^{\circ}\text{C}$  and  $80^{\circ}\text{C}$ .
- [2.3.3.9] The system operates without malfunction with environmental humidity ranging between 5% and 95%.
- [2.2.3.10] Each MPPT communicates with the vehicle via the vehicle's CAN-bus on a send-only basis, providing (next to all communication necessary for safe and reliable CAN-bus operation) at least: power in [W], power out [W], input voltage [V], output voltage [V], output current [A].
- [2.2.3.11] The MPPT has at least 4 status LEDs, showing operating status and/or possible error codes.
- [2.2.3.12] The MPPT provides In-System Programming (ISP) using a JTAG interface.
- [2.2.3.13] All components meet the specifications as provided by Veolia World Solar Challenge.
- [2.2.3.14] High-voltage connections must be properly shielded.
- [2.2.3.15] All critical high-power connections contain correctly dimensioned fuses.
- [2.2.3.16] Casings and enclosures must be constructed properly and provide adequate sealing, strength and durability to protect enclosed components.
- [2.2.3.17] All connections will be dust-sealed, shock and vibration proof.

#### **Production and installation requirements**

- [2.3.4.1] The MPPT and all its components are integrated in a enclosure for easy mounting in the Nuna 6.
- [2.3.4.2] Installation of the system is possible using standard tools available to the Nuon Solar team.

- [2.3.4.3] Each enclosure has a label for identification purposes.
- [2.3.4.4] External connections provide standard connectors for easy installation in the vehicle: power bus connectors: Green Power Connector PC 4 HV/4-STF-7.62 Phoenix, CAN-bus connectors: Orange CAN Connector BL 3,5/4 Weidmüller.

**Requirements on product end-of-life**

- [2.2.5.1] The MPPT complies with EU WEEE guidelines for electronic waste disposal.
- [2.2.5.2] The system must be removable from the vehicle.
- [2.2.5.3] Any batteries in the system must be easy to remove to be processed separately.

**Strategic and marketing requirements**

- [2.2.6.1] The system is sold business-to-business.



# Appendix D - IRFSL4620

## Efficiency Measurements

LOAD RESISTANCE: 100.02 Ohm      MOSFET: IRFSL4620      LOSSES IN DRIVER AND MICRO: 10V @ 0,02A = 0,2W

DUTYCYCLE	IN VOLTAGE	IN CURRENT	OUT VOLTAGE	OUT CURRENT	LOAD RESISTANCE	POWER IN	POWER OUT	POWER DISS	EFFICIENCY
20%	50,00	0,80	61,80	0,63	98,4	40,23	38,81	1,42	96,47%
	55,00	0,88	68,05	0,69	98,3	48,65	47,09	1,55	96,80%
	60,00	0,96	74,30	0,76	98,3	57,90	56,17	1,73	97,01%
	65,00	1,04	80,54	0,82	98,3	67,97	65,96	2,00	97,05%
	70,00	1,12	86,83	0,88	98,3	78,84	76,67	2,17	97,25%
	80,00	1,30	98,70	1,03	95,5	104,32	102,00	2,32	97,77%
	90,00	1,46	111,10	1,16	96,1	131,40	128,39	3,01	97,71%
	100,00	1,63	123,80	1,30	95,5	163,00	160,57	2,43	98,51%
	110,00	1,81	136,20	1,43	95,2	198,55	194,90	3,65	98,16%
	120,00	1,97	148,50	1,57	94,9	236,88	232,40	4,48	98,11%
30%	50,00	1,05	70,68	0,72	98,2	52,75	50,89	1,86	96,47%
	55,00	1,16	77,82	0,79	98,5	63,83	61,48	2,35	96,32%
	60,00	1,26	84,92	0,86	98,7	75,90	73,03	2,87	96,22%
	65,00	1,37	92,13	0,94	98,3	89,35	86,33	3,02	96,62%
	70,00	1,47	99,27	1,01	98,3	103,48	100,26	3,22	96,89%
	80,00	1,73	113,30	1,19	95,1	138,40	135,05	3,35	97,58%
	90,00	1,95	127,70	1,34	95,4	175,32	170,99	4,33	97,53%
	100,00	2,16	141,90	1,49	95,2	216,17	211,43	4,74	97,81%
	110,00	2,39	156,40	1,65	95,1	262,35	257,28	5,07	98,07%
	120,00	2,61	170,90	1,80	95,0	312,96	307,45	5,51	98,24%
40%	50,00	1,43	82,51	0,84	98,2	71,85	69,31	2,54	96,46%
	55,00	1,58	90,87	0,93	98,2	86,98	84,05	2,93	96,64%
	60,00	1,72	99,18	1,00	99,2	103,50	99,18	4,32	95,83%
	65,00	1,87	107,61	1,10	98,1	121,79	118,05	3,74	96,93%
	70,00	2,01	115,85	1,18	98,2	141,28	136,70	4,58	96,76%
	80,00	2,35	132,00	1,39	95,0	187,76	183,35	4,41	97,65%
	90,00	2,64	148,40	1,56	95,0	237,69	231,80	5,89	97,52%
	100,00								
	110,00								
	120,00								
50%	50,00	2,06	99,18	1,01	98,5	103,20	99,87	3,33	96,78%
	55,00	2,27	109,20	1,11	98,5	124,99	121,10	3,88	96,89%
	60,00	2,48	119,17	1,21	98,4	148,86	144,31	4,55	96,95%
	65,00	2,68	129,07	1,31	98,4	174,50	169,34	5,16	97,04%
	70,00	2,90	139,03	1,42	98,0	203,30	197,28	6,02	97,04%
60%	50,00	3,20	123,90	1,26	98,3	160,45	156,24	4,21	97,37%